Australian Government
Geoscience Australia

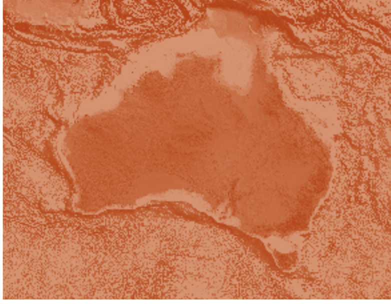

Geoscience Australia Record 2013/25 | **GeoCat** 76362
Mineral Resources Authority of Papua New Guinea Technical Note TN 2013/05

New SHRIMP U-Pb zircon ages from the Wau-Bulolo region, Papua New Guinea

July 2012–June 2013

S. Bodorkos, S. Sheppard, D. Saroa, C.U. Tsiperau and K.N. Sircombe

Mineral Resources Authority

New SHRIMP U-Pb zircon ages from the Wau-Bulolo region, Papua New Guinea

July 2012–June 2013

GEOSCIENCE AUSTRALIA
RECORD 2013/25

MINERAL RESOURCES AUTHORITY, PAPUA NEW GUINEA
TECHNICAL NOTE TN 2013/05

S. Bodorkos[1], S. Sheppard[2,3], D. Saroa[2], C.U. Tsiperau[2] and K.N. Sircombe[1]

Australian Government
Geoscience Australia

Mineral Resources Authority

1. Minerals and Natural Hazards Division, Geoscience Australia, GPO Box 378, Canberra ACT 2601 AUSTRALIA
2. Mineral Resources Authority, PO Box 1906, Port Moresby, National Capital District 121, PAPUA NEW GUINEA
3. Now at: Brockman Mining Limited, Level 1, 117 Stirling Highway, Nedlands WA 6009, AUSTRALIA

Australian Department of Resources, Energy and Tourism

Minister for Resources and Energy: The Hon. Gary Gray AO MP
Secretary: Mr Blair Comley, PSM

Geoscience Australia
Chief Executive Officer: Dr Chris Pigram

Papua New Guinea Department of Mining
Minister for Mining: The Hon. Byron Chan, MP

Mineral Resources Authority of Papua New Guinea
Acting Managing Director: Mr Philip Samar
Acting Executive Manager, Geological Survey Division: Mr Nathan Mosusu

This paper is published with the permission of the CEO, Geoscience Australia, and the Executive Manager, Geological Survey Division, Mineral Resources Authority of Papua New Guinea.

ISSN 2201-702X (PDF)

ISBN 978-1-922201-57-7 (PDF)

GeoCat 76362

Bibliographic reference: Bodorkos, S., Sheppard, S., Saroa, D., Tsiperau, C.U. & Sircombe, K.N., 2013. *New SHRIMP U-Pb zircon ages from the Wau-Bulolo region, Papua New Guinea*. Geoscience Australia Record 2013/25; Mineral Resources Authority, Papua New Guinea, Technical Note TN 2013/05. Geoscience Australia, Canberra.

Version: 1308

Contents

Executive Summary

This report presents new zircon U-Pb geochronological data obtained via Sensitive High Resolution Ion Micro Probe (SHRIMP) from rocks sampled within the Wau 1:100 000 map sheet area, which is located on the Papuan Peninsula in eastern Papua New Guinea. Exposure in the Wau-Bulolo region comprises low-grade Mesozoic metasedimentary rocks of the Owen Stanley Metamorphics, which are intruded by the mid-Miocene Morobe Granodiorite batholith, and overlain by Pliocene sedimentary and volcanic rocks of the Wau Basin. The map sheet area contains the Morobe Goldfield (from which more than 3.2 Moz of alluvial gold has been mined) and the Hidden Valley epithermal Au-Ag deposit (which has a total gold resource in excess of 3 Moz), and lies about 70 km south-southeast of the giant mid-Miocene Wafi-Golpu porphyry Cu-Au deposit (in excess of 26 Moz Au and 9 Mt Cu).

The geochronological data in this report were generated as part of a collaborative project between Geoscience Australia (GA) and the Mineral Resources Authority (MRA) of Papua New Guinea in 2012. Four samples were analysed: two from the Pliocene Bulolo Volcanics and one from the Miocene Morobe Granodiorite to establish precise, accurate magmatic crystallisation ages, and one metasandstone from the Mesozoic Owen Stanley Metamorphics for detrital zircon provenance analysis. Sample locations, descriptions, and U-Pb SHRIMP results are summarised in Table 1.1.

The two samples from the Bulolo Volcanics bracket the age of the eruptive event. One sample is an andesite ‘bomb’ hosted by volcanic breccia, and its magmatic crystallisation age of 3.46 ± 0.06 Ma defines a maximum age for breccia deposition, although the evidence for high-temperature emplacement of bombs within this exposure suggests that the host breccia was deposited at about the same time as the ‘bomb’ crystallised. The other sample is a subvolcanic diorite, and its magmatic crystallisation age of 3.22 ± 0.06 Ma defines a minimum age for the host Bulolo Volcanics breccia it intrudes. The two dates are distinct at the 95% confidence level (MSWD = 32, P_{equiv} = 0.000), and indicate that the Bulolo Volcanics were deposited between 3.46 ± 0.06 Ma and 3.22 ± 0.06 Ma: an interval of 0.24 ± 0.08 million years. Both results are in excellent agreement with a plagioclase K-Ar isochron age of 3.39 ± 0.22 Ma determined for the Bulolo Volcanics by Page and McDougall (1972).

The Morobe Granodiorite was sampled in the western Kuper Range, and yielded a magmatic crystallisation age of 13.62 ± 0.13 Ma, which is slightly older than a hornblende K-Ar age of c. 12.6 Ma in the Kuper Range about 2 km to the north, and hornblende and biotite K-Ar ages of c. 12.3 Ma and c. 11.0 Ma from the Ekuti Range south of Wau (Page, 1976). However, the new U-Pb age is consistent with a larger body of isotopic data from the Watut, Sunshine and Gurukar plutons (distributed along the Sunshine Fault; Page, 1976), comprising K-Ar isochron ages of 14.8 ± 1.3 Ma (hornblende) and 13.2 ± 0.7 Ma (biotite), and biotite Rb-Sr ages spanning the range 14.5–12.7 Ma. The agreement of the new U-Pb age with the multi-sample K-Ar and Rb-Sr results suggests that all five plutons of the Morobe Granodiorite are the same age. The sample collected for SHRIMP U-Pb geochronology also yielded inherited zircon ages of c. 234 Ma and c. 187 Ma, which are similar to U-Pb zircon dates, K-Ar isochrons and Rb-Sr dates for Triassic and Jurassic plutons exposed some 200–500 km to the northwest (Page, 1976; Van Wyck and Williams, 2002).

The zircon-bearing metasandstone sample from the Owen Stanley Metamorphics is dominated by Permian detritus, with 65 of 115 analyses yielding ages between c. 300 Ma and c. 265 Ma. The

median age of this group (282.6 +1.7/-1.3 Ma) is a conservative estimate of the maximum age of deposition of the precursor sandstone. A further 38 analyses yielded a diverse range of Late Carboniferous (c. 310 Ma) to Neoarchean (c. 2804 Ma) ages, with only one statistically significant cluster of five analyses at c. 1551 Ma. Most of the detrital ages are well matched to felsic igneous sources in northeastern Australia, including the Late Paleozoic New England Orogen and Drummond Basin, the Neoproterozoic–Devonian Thomson Orogen, and the Paleo-Mesoproterozoic Coen, Georgetown and Mount Isa provinces (e.g. Carson et al., 2006, 2011; Neumann and Fraser, 2007; Cross et al., 2009, 2012, and references therein). The new U-Pb detrital zircon age spectrum from the Owen Stanley Metamorphics spectrum strongly resembles one previously obtained from the Omung Metamorphics some 220 km to the northwest (Van Wyck and Williams, 2002), which raises the possibility that protoliths of the Omung Metamorphics form part of the Owen Stanley Metamorphics. If so, the minimum age for the former (provided by the c. 240 Ma Kubor Granodiorite) would explain the absence of mid-Triassic and younger zircons from the provenance spectrum of the Owen Stanley Metamorphics, despite post-230 Ma felsic rocks being widespread in the proposed source region (e.g. Carson et al., 2006; Cross et al., 2009, 2012).

1. Introduction

Many aspects of the geology and tectonic evolution of Papua New Guinea remain poorly understood. This is partly a function of the extensive rainforest cover, rugged terrain and lack of infrastructure; however, it is also related to the paucity of publicly available data, including robust geochronological and isotopic data, for many rock units. Some of these gaps in the Wau-Bulolo region (which is one of the most prospective areas in Papua New Guinea for epithermal and porphyry deposits) were addressed by geological mapping and sampling conducted by the Mineral Resources Authority of Papua New Guinea (MRA) in 2011, the results of which are summarised by Saroa et al. (2012).

This report contains new zircon U-Pb geochronological data obtained via Sensitive High-Resolution Ion Micro Probe (SHRIMP) from three volcanic and plutonic igneous rocks and one metasedimentary rock from the Wau 1:100 000 map sheet area, in eastern Papua New Guinea (Figure 1.1). These data were obtained during the reporting period July 2012–June 2013, under the auspices of a collaborative Geochronology Project between MRA and Geoscience Australia (GA), and the results are summarised in Table 1.1.

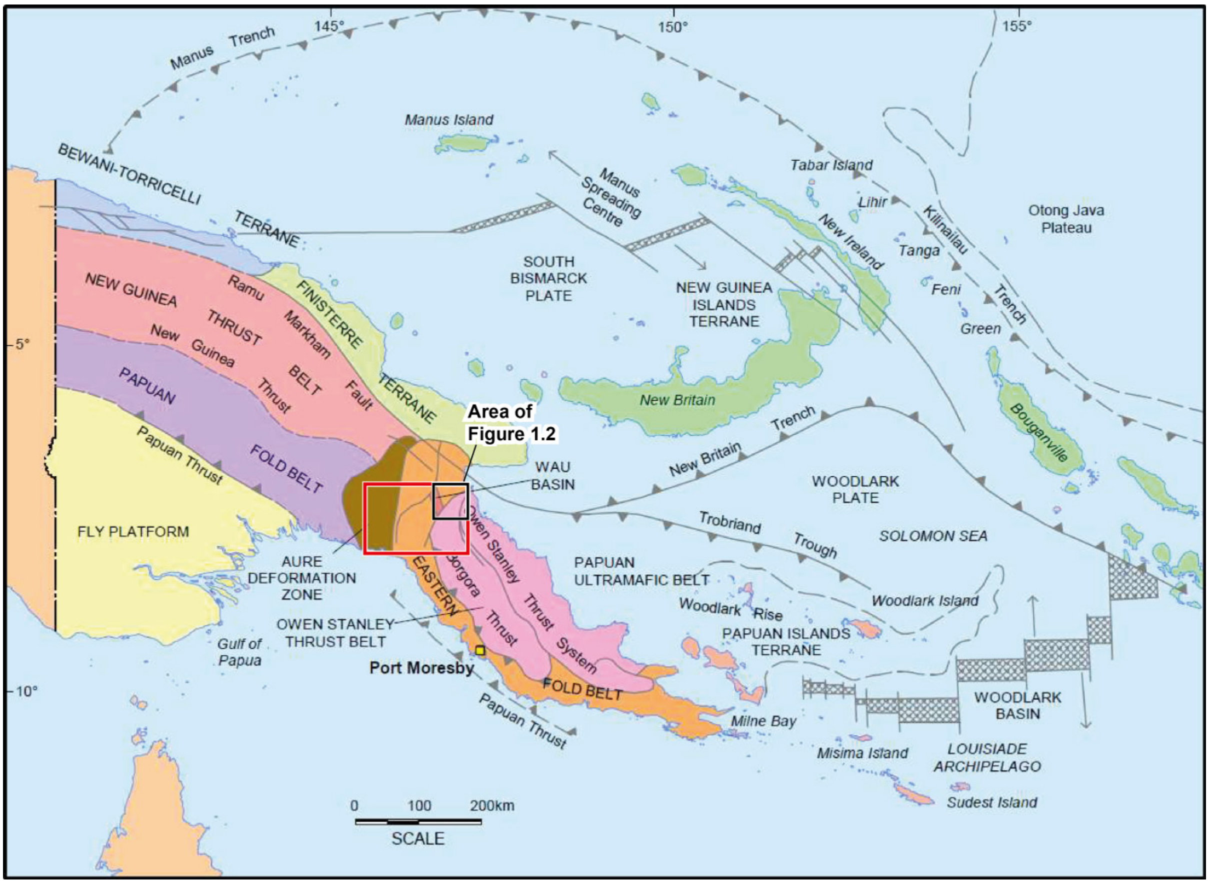

Figure 1.1 *Major geological elements of Papua New Guinea and its environs, modified from Williamson and Hancock (2005). The red rectangle and the black square respectively define the locations and extents of the Wau 1:250 000 (Dow et al., 1974) and Wau 1:100 000 map sheets. The geology of the latter is depicted in Figure 1.2.*

1.1. Geological Overview

The Wau 1:100 000 map sheet area is situated on the southeast-trending Papuan Peninsula, the greater part of which is underlain by the Owen Stanley Metamorphics (Figure 1.1). This metamorphic complex is nearly 400 km long and 80 km wide, and comprises two belts: a western belt of very low-grade rocks and an eastern belt of higher grade rocks with evidence of high-pressure metamorphism. The western belt consists of argillite, shale, lithic and feldspathic sandstone, greywacke with minor limestone, conglomerate and spilitic volcanic rocks, whereas the eastern belt is composed of phyllite, slate, pelitic and psammitic schist, and lesser metavolcanic rock, with blueschist and granulite close to the Owen Stanley Fault System and the overthrust Papuan Ultramafic Belt (Pieters, 1978; Rogerson and Francis, 1983; Pigram and Davies, 1987; Worthing, 1988). Protoliths of the Owen Stanley Metamorphics were fine-grained marine sediments deposited as a thick pile on the rifted margin of northern Australia, possibly during the Cretaceous, based on the presence of macrofossils of Aptian–Cenomanian age in the western part of the succession (Dow et al., 1974).

Metamorphic rocks of the Owen Stanley Metamorphics are intruded by Oligocene gabbro and by Miocene granites, including the mid-Miocene Morobe Granodiorite (Fisher, 1944), and overlain by late Oligocene and younger volcanic and sedimentary rocks, including those of the Wau Basin. The Morobe Granodiorite comprises about 3500 km^2 of medium-grained granodiorite, locally with monzogranite and monzonite (Fisher, 1944; Mackay, 1955; Carswell, 1990). The Wau Basin is a north-northwest-trending depression about 40 km long and 20 km wide that formed during the Pliocene. Volcanic and sedimentary rocks of the basin were deposited nonconformably on the Owen Stanley Metamorphics and the Morobe Granodiorite.

1.2. Samples Analysed

The samples selected for analysis were obtained from three discrete geological units (Figure 1.2):

- Two from the Bulolo Volcanics in the Wau Basin. One (MRA 100214) comprises ‘bombs’ of porphyritic andesite hosted by volcanic breccia about 6.5 km north of Wau; the other (MRA 100338) is a diorite intruding the volcanic breccia about 6.5 km north-north west of Edie Creek.
- One from the Morobe Granodiorite, comprising an inclusion-rich granodiorite (MRA 100417) from the western Kuper Range, about 4 km east-southeast of Sam Sam No 1 village.
- Two from the Owen Stanley Metamorphics, both obtained from thin layers of foliated metasandstone hosted by sheared dark blue-grey phyllite. Zircons were obtained from the western sample (MRA 100211), collected about 3 km west of Wau, but not from the eastern sample (MRA 100215) collected about 2 km north-northeast of Elaru village.

This report documents detailed results for each sample, encompassing location and description, geological context, zircon descriptions, an evaluation of the relevant analytical data, and a brief geochronological interpretation. This is followed by a brief Discussion of the new SHRIMP U-Pb results in the context of existing isotopic data for each unit. The results are summarised in Table 1.1, and are available via GA’s Geochron Delivery system (http://www.ga.gov.au/geochron-sapub-web/).

A comprehensive description of sample acquisition and processing procedures, preparation and analysis of SHRIMP mounts, and data reduction and presentation methods are included in the Appendix, along with analytical session-specific details of the calibration data collected on the reference $^{238}U/^{206}Pb$ and $^{207}Pb/^{206}Pb$ zircons.

Table 1.1 *Summary of sample descriptions, locations, and SHRIMP U-Pb ages for the MRA–GA Geochronology Project 2012–13 (Wau–Bulolo region, Papua New Guinea). Eastings and northings lie within Universal Transverse Mercator (UTM) Zone 55.*

MRA SampleNo	GA SampleNo	Stratigraphic Unit and Description	WGS84 Easting	WGS84 Northing	WGS84 Latitude	WGS84 Longitude	Interpreted $^{238}U/^{206}Pb$ Age (±95% confidence)	Comments
100214	2131308	Bulolo Volcanics: andesite 'bombs' within volcanic breccia. About 6.5 km north of Wau.	468633	9194460	-7.287490	146.715834	3.46 ± 0.06 Ma (29 analyses)	Magmatic crystallisation age. Eight analyses yielded inherited ages between c. 4.4 Ma and c. 987 Ma.
100338	2131310	Bulolo Volcanics: subvolcanic diorite intruding volcanic breccia. About 6.5 km northwest of Edie Creek.	458755	9191036	-7.318398	146.626320	3.22 ± 0.06 Ma (32 analyses)	Magmatic crystallisation age. Three analyses yielded inherited ages between c. 3.6 Ma and c. 51 Ma.
100417	2131311	Morobe Granodiorite: inclusion-rich granodiorite. About 4 km east-southeast of Sam Sam No 1 village.	459772	9216442	-7.088590	146.635718	13.62 ± 0.13 Ma (27 analyses)	Magmatic crystallisation age. Seven analyses yielded inherited ages between c. 14.7 Ma and c. 397 Ma.
100211	2131307	Owen Stanley Metamorphics: foliated metasandstone. About 3 km west of Wau.	465869	9189116	-7.335814	146.690760	282.6 +1.7/-1.3 Ma (65 analyses between c. 300 Ma and c. 265 Ma)	Maximum age for deposition of precursor sandstone. Thirty-eight analyses yielded older provenance ages between c. 310 Ma and c. 2804 Ma.
100215	2131309	Owen Stanley Metamorphics: foliated metasandstone. About 2 km north-northeast of Elaru village.	477231	9182209	-7.398352	146.793674	—	No zircon found.

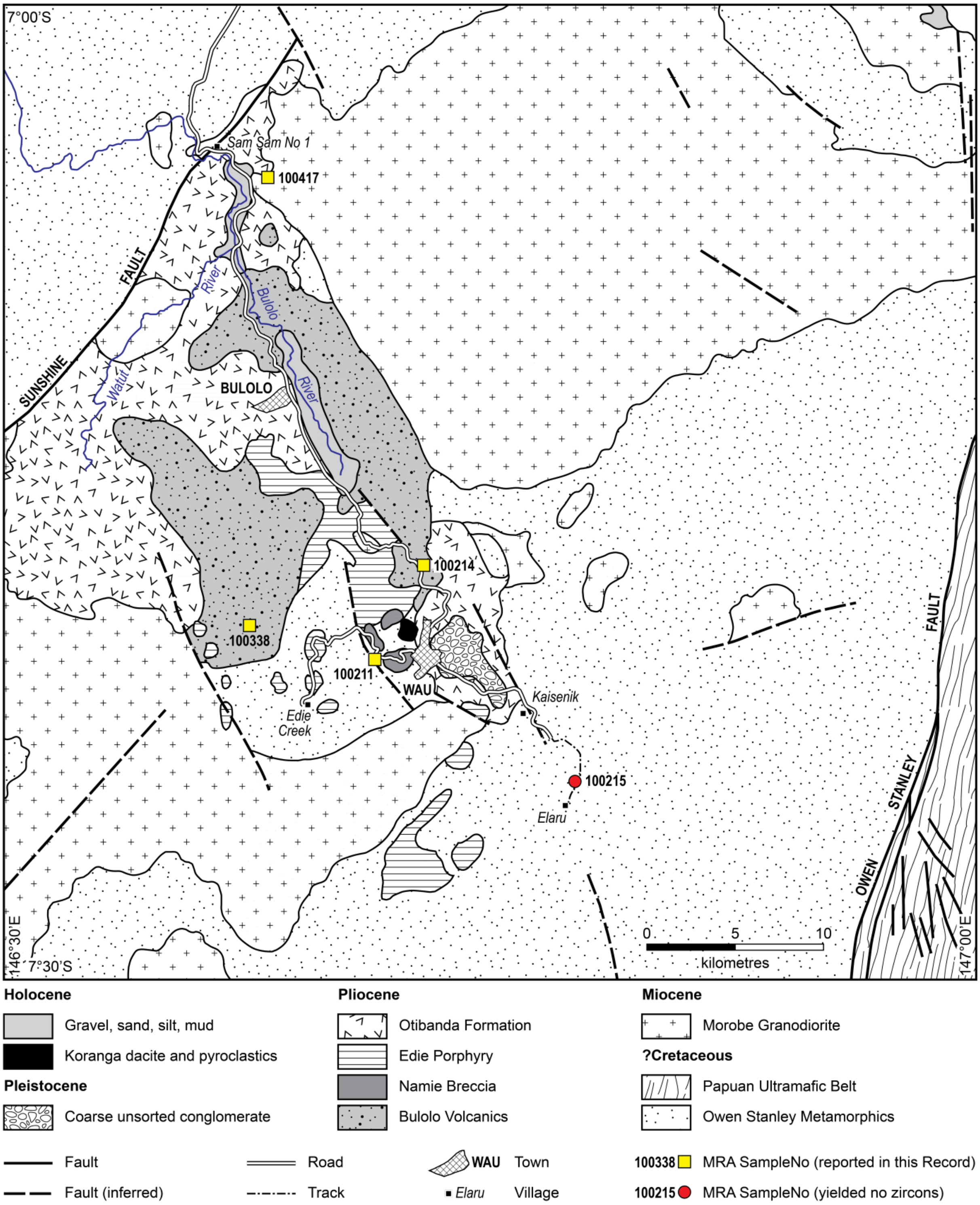

***Figure 1.2** Interpreted bedrock geology of the Wau 1:100 000 map sheet area (simplified from Dow et al., 1974), showing locations of the five samples (labelled with MRA SampleNo) targeted for SHRIMP U-Pb zircon analysis. See Figure 1.1 for location.*

2. Bulolo Volcanics

The Bulolo Volcanics is confined to the Wau Basin, and mainly comprises volcanic breccia and conglomerate, volcaniclastic sandstone, and andesitic and dacitic lava and syn-volcanic intrusions (Saroa et al., 2012). The Bulolo Volcanics is nonconformable on the Owen Stanley Metamorphics, Morobe Granodiorite and Edie Porphyry (Plane, 1967), although in the Wau area, the Edie Porphyry also intrudes the Bulolo Volcanics. The Bulolo Volcanics is overlain conformably by the Otibanda Formation (Plane, 1967; Dow et al., 1974; Sillitoe et al., 1984), although Cussen et al. (1986) noted interfingering of the Bulolo Volcanics with the Otibanda Formation, mainly in the Bulolo area. Several K-Ar determinations by Page and McDougall (1972) on biotite and plagioclase from volcanic rocks in the Bulolo Volcanics yielded ages of about 3.5 Ma.

2.1. Andesite 'bombs' within breccia, Bulolo Volcanics

Table 2.1 *Summary of results: andesite 'bombs', Bulolo Volcanics (MRA 100214, GA 2131308).*

MRA SiteID	CUT000021
MRA SampleNo	100214
GA SampleNo	2131308
Lithology	Porphyritic andesite 'bombs' within volcanic breccia
Stratigraphic Unit	Bulolo Volcanics
1:250 000 Sheet	WAU (SB55-14)
1:100 000 Sheet	WAU (8283)
WGS84 Location (Geographic)	7.287490°S, 146.715834°E
WGS84 Location (UTM Zone 55)	468633 mE, 9194460 mN
Analytical Session(s)	120071 (see Appendix Table A.1 for parameters derived from measurements of $^{238}U/^{206}Pb$ and $^{207}Pb/^{206}Pb$ reference zircons)
Interpreted Age	3.46 ± 0.06 Ma (95% confidence; 29 analyses of 29 zircons)
Geological Attribution	Magmatic crystallisation
Isotopic Ratio(s) Used	$^{238}U/^{206}Pb$ (^{207}Pb-corrected)

2.1.1. Sampling Details, Rock Description and Geological Relationships

This sample was collected about 6.5 km north of the town of Wau, from an exposure in a road cut along the forestry bypass road between Pinetop and Wau.

The unit sampled for geochronology consists of two bombs, each about 25 cm in diameter, within a volcanic breccia. The bombs (which show 'necking', and probably represent a larger bomb that has been pulled apart) are sparsely porphyritic andesite, and comprise about 5% euhedral plagioclase phenocrysts 1.0–1.5 mm long, set in a strongly recrystallised groundmass of albitic plagioclase, chlorite, calcite, sericite and very fine-grained granular epidote and titanite. Other breccia-hosted bombs in the same outcrop also show evidence of high-temperature emplacement, such as chilled and crenulate margins, sac shapes, and bombs flattened against each other (Figure 10 of Saroa et al., 2012).

The host volcanic breccia is interpreted as a pyroclastic deposit occurring near the stratigraphic top of the Bulolo Volcanics. This sample, in conjunction with sample MRA 100338 (GA 2131310), was analysed in an attempt to better constrain the age of eruption of the Bulolo Volcanics.

2.1.2. Zircon Description

The mounted crystals are moderately to strongly elongate, with long axes and aspect ratios (length/width) spanning the ranges 50–380 μm and 1–5, respectively (Figure 2.1). Crystal forms are euhedral to subhedral, and external morphologies dominated by faceted prismatic grains with well-developed pyramidal terminations. In transmitted light, the crystals are predominantly transparent and colourless to pale pink. Most grains host inclusions of pale- and dark-coloured minerals (Figure 2.1). In many crystals, a contrast is evident in transmitted light between older, mostly inclusion-rich inherited cores and younger, largely inclusion-free pyramidal overgrowths. Core-rim interfaces are commonly demarcated by clusters of very fine-grained, dark-coloured mineral inclusions.

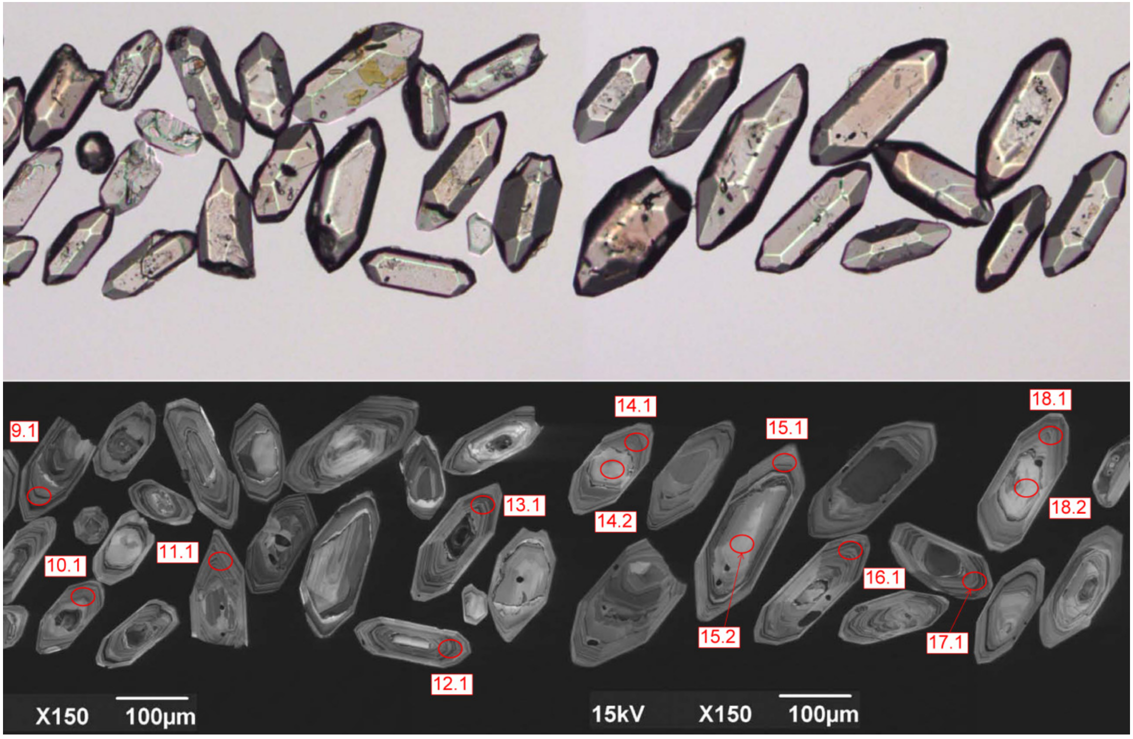

***Figure 2.1** Representative zircons from the andesite 'bombs', Bulolo Volcanics (MRA 100214, GA 2131308). Transmitted-light image is shown in the upper half; cathodoluminescence image in the lower half. SHRIMP analysis sites are indicated, and labelled with grain and area number.*

Cathodoluminescence (CL) images reveal moderate to high CL emission intensities, and predominantly margin-parallel oscillatory zoning patterns. Most crystals are characterised by core regions with relatively indistinct zoning patterns and CL emission intensities that vary widely from grain to grain. Zoning in the cores is invariably truncated by disconformable pyramidal terminations, with uniformly high CL emission and moderate-contrast oscillatory zoning (Figure 2.1). The uniform appearance of the pyramidal overgrowths means it is likely that they represent magmatic crystallisation of the host porphyritic andesite, with the heterogeneous core regions reflecting a variety of older zircons inherited by the andesite magma.

2.1.3. U-Pb Isotopic Results

Thirty-seven analyses were obtained from 32 zircon crystals, and the results are presented in Figures 2.2–2.3 and Table 2.2. Five grains (1, 3, 14, 15 and 18) were each analysed twice. The analyses are characterised by a wide range of U contents (80–1358 ppm, median 460 ppm), predominantly low to moderate Th/U (0.14–1.02, median 0.41), and mostly low $^{206}Pb_c$ (maximum 3.76%, median 0.50%). They can be divided into three groups (Table 2.2) based on textural and isotopic criteria:

- Group 1 comprises 29 analyses of 29 zircons, predominantly sited within euhedral pyramidal terminations with concentric oscillatory zoning, many of which have disconformably overgrown inherited cores (Figure 2.1). Their individual ^{207}Pb-corrected $^{238}U/^{206}Pb$ dates range between c. 3.85 Ma and c. 3.19 Ma (Figures 2.2–2.3), and define a weighted mean date of 3.45 ± 0.06 Ma (95% confidence), although the scatter of the constituent analyses significantly exceeds that expected from the individual analytical uncertainties (MSWD = 4.1, P_{equiv} = 0.000).
- Group 2 comprises three analyses of three zircons, sited within crystals with concentric oscillatory zoning from centre to edge (Figure 2.1). Their individual ^{207}Pb-corrected $^{238}U/^{206}Pb$ dates range between c. 12.5 Ma and c. 4.4 Ma (Figures 2.2–2.3).
- Group 3 comprises five analyses of five zircons, each sited within an inherited core characterised by the disconformable overgrowth of at least one euhedral oscillatory-zoned pyramidal termination (Figure 2.1). Their individual ^{204}Pb-corrected $^{238}U/^{206}Pb$ dates range between c. 987 Ma and c. 181 Ma (Figures 2.2–2.3).

2.1.4. Geochronological Interpretation

The weighted mean ^{207}Pb-corrected $^{238}U/^{206}Pb$ date of 3.45 ± 0.06 Ma (95% confidence) obtained from the 29 analyses in Group 1 is interpreted as an estimate of the magmatic crystallisation age of the andesite 'bombs' within the volcanic breccia, even though the scatter of the constituent analyses (MSWD = 4.1, P_{equiv} = 0.000) exceeds that expected from the individual analytical uncertainties.

Ordinarily, this would indicate that the statistical coherence of the 29 analyses in Group 1 is compromised by geological sources of variation, such as the inclusion of analyses with individual $^{238}U/^{206}Pb$ dates that are 'pre-magmatic' (e.g. sampling marginally older inherited zircons) and/or 'post-magmatic' (e.g. sampling zircon domains affected by post-crystallisation loss of radiogenic Pb). In this case, however, the probability density distribution (Figure 2.3) is quite symmetrical about its maximum value, and the intrinsically asymmetric 95% confidence interval on the median $^{238}U/^{206}Pb$ date for Group 1 (3.46 +0.03/-0.03 Ma) displays similar symmetry.

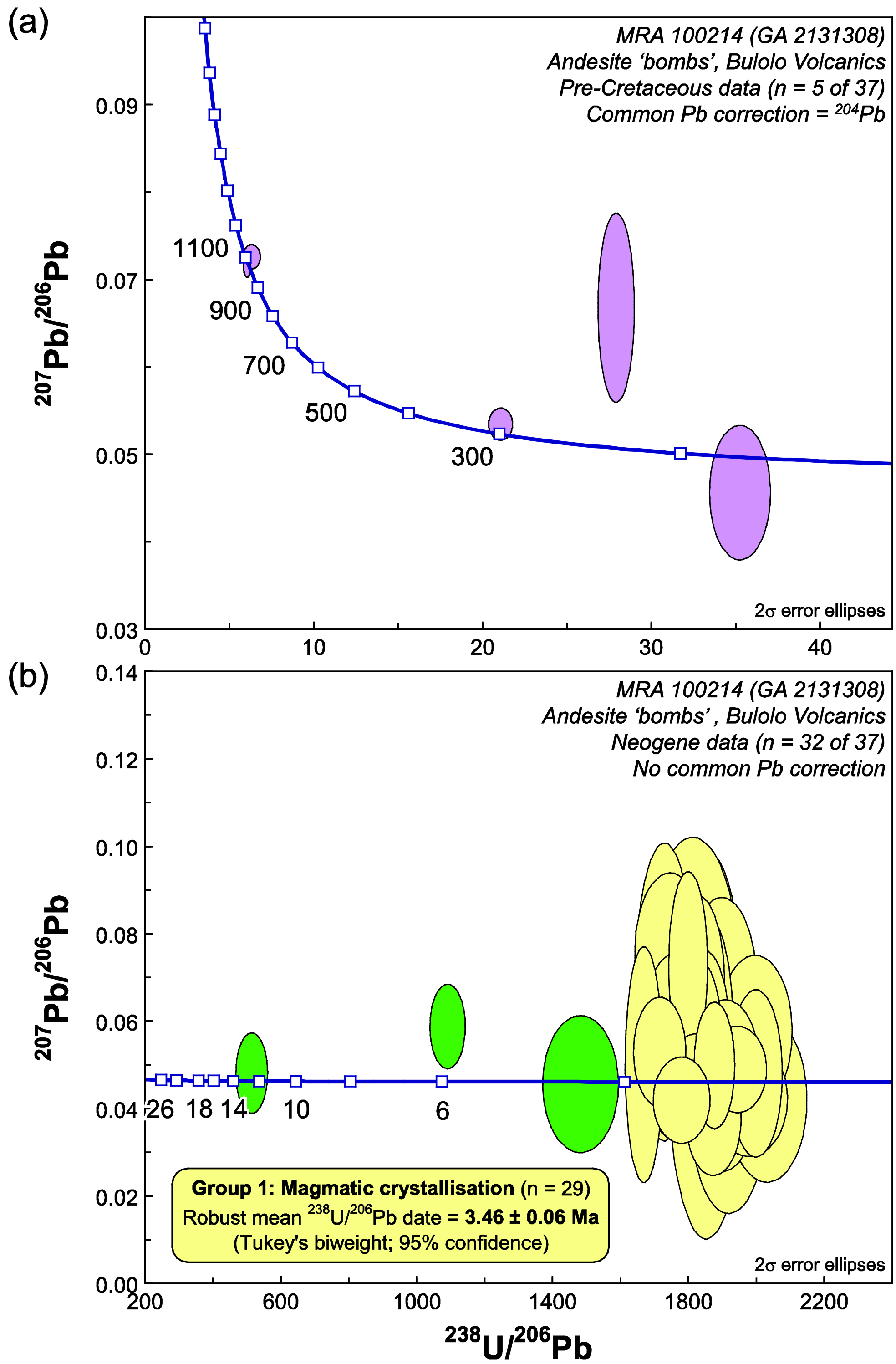

Figure 2.2 *Tera-Wasserburg concordia diagrams for SHRIMP U-Pb zircon data from the andesite 'bombs', Bulolo Volcanics (MRA 100214, GA 2131308). (a) Pre-Cretaceous data; (b) Neogene data. Pale yellow fill denotes Group 1 (magmatic crystallisation); green fill denotes Group 2 (Miocene–Pliocene inheritance); pink fill denotes Group 3 (pre-Cretaceous inheritance).*

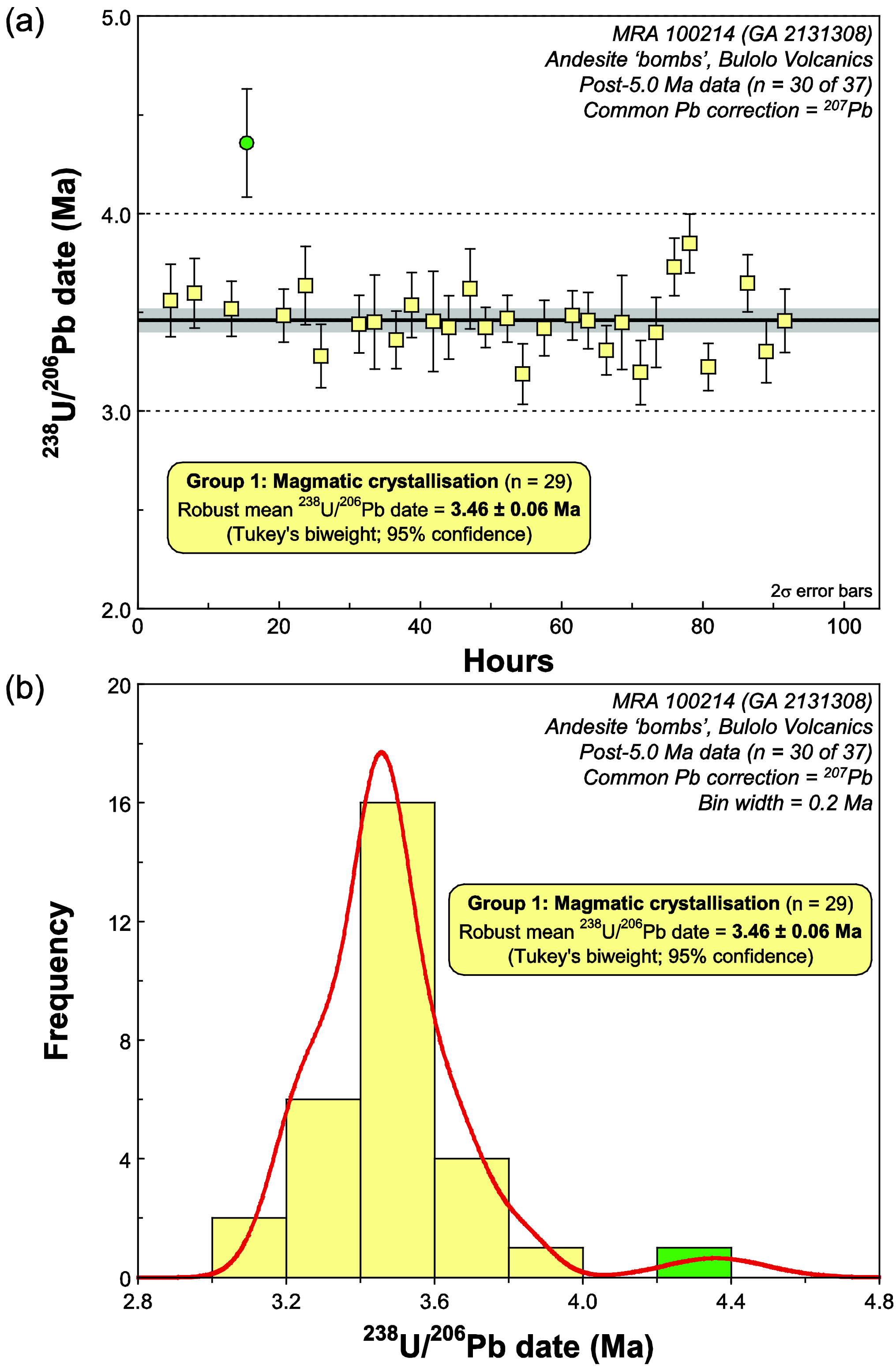

Figure 2.3 *Post-5.0 Ma analyses from the andesite 'bombs', Bulolo Volcanics (MRA 100214, GA 2131308). (a) Individual $^{238}U/^{206}Pb$ dates in order of acquisition; (b) Frequency histogram and probability density distribution. Pale yellow fill denotes Group 1 (magmatic crystallisation); green fill denotes Group 2 (Miocene–Pliocene inheritance). Heavy black line and grey band: weighted mean $^{238}U/^{206}Pb$ date and its 95% confidence interval; red curve: relative probability density distribution.*

These observations suggest that if the observed scatter is truly geological in origin, then analyses of inherited zircon and zircon affected by loss of radiogenic Pb must be present in Group 1 in roughly equal proportions. This seems unlikely, so it is possible that the apparent scatter of the analyses in Group 1 is non-geological. For example, the effect of very low count rates measured by SHRIMP at mass ^{206}Pb in Pliocene zircons with only moderate U contents (median c. 11 counts per second for the 29 analyses in Group 1) may have been underestimated by the data-processing software, resulting in individual ^{238}U/^{206}Pb analyses being assigned uncertainties that are too small. Consequently, a mean ^{207}Pb-corrected ^{238}U/^{206}Pb date for Group 1 (Figure 2.3) is most appropriately calculated using the robust Tukey's Biweight method (Hoaglin et al., 1983, implemented by Ludwig, 2009), which ignores the uncertainties assigned to the individual analyses, and instead weights the analyses according to their scatter from an (iteratively-determined) mean.

The resulting robust mean ^{207}Pb-corrected ^{238}U/^{206}Pb date for the 29 analyses in Group 1 is 3.46 ± 0.06 Ma, which is interpreted as the best estimate of the magmatic crystallisation age of the porphyritic andesite 'bombs'. Based on the field evidence for high-temperature emplacement of bombs at the sample locality, the robust mean date of 3.46 ± 0.06 Ma also represents the best estimate of the eruption age of the host volcanic breccia, which lies near the stratigraphic top of the Bulolo Volcanics. The three analyses in Group 2 are interpreted to reflect 'pre-magmatic' xenocrystic or antecrystic zircons of Miocene to Pliocene age, and the five analyses in Group 3 are interpreted to represent inherited cores ranging in age from Neoproterozoic to Jurassic.

***Table 2.2** SHRIMP U-Pb zircon data from the andesite 'bombs', Bulolo Volcanics (MRA 100214, GA 2131308). Unless otherwise indicated in the Group heading, all isotopic ratios are uncorrected for common Pb and all dates are ^{207}Pb-corrected ^{238}U/^{206}Pb.*

Grain.area .replicate	$^{206}Pb_c$ (%)	U (ppm)	Th (ppm)	^{232}Th /^{238}U	^{238}U /^{206}Pb	±1σ (%)	^{207}Pb /^{206}Pb	±1σ (%)	Date (Ma)	±1σ (Ma)	Disc (%)
Group 3: Pre-Cretaceous inheritance (n = 5; isotopic ratios, dates and discordance are ^{204}Pb-corrected)											
1.2.1	-0.05	490	138	0.29	6.05	1.36	0.07135	0.66	986.7	13.0	-2
3.2.1	0.21	353	109	0.32	6.32	3.23	0.07254	0.78	945.5	29.5	6
18.2.1	0.06	566	119	0.22	21.05	1.42	0.05350	1.38	298.8	4.2	15
15.2.1	0.40	80	41	0.53	27.89	1.58	0.06670	6.59	222.6	3.4	74
14.2.1	0.08	104	102	1.02	35.24	2.09	0.04572	6.85	181.3	3.7	—
Group 2: Miocene–Pliocene inheritance (n = 3)											
3.1.1	0.25	395	94	0.25	514	3.6	0.04823	7.7	12.49	0.46	—
6.1.1	1.60	838	466	0.58	1089	1.9	0.05883	6.7	5.82	0.12	—
5.1.1	-0.05	444	118	0.27	1479	3.0	0.04571	13.9	4.36	0.14	—
Group 1: Magmatic crystallisation (n = 29)											
28.1.1	0.50	237	89	0.39	1666	1.3	0.05008	21.8	3.85	0.07	—
27.1.1	0.87	917	473	0.53	1713	1.8	0.05301	9.6	3.73	0.07	—
30.1.1	-0.52	1198	172	0.15	1776	1.9	0.04204	9.5	3.65	0.07	—
8.1.1	2.60	356	176	0.51	1726	2.1	0.06665	20.7	3.64	0.10	—
16.1.1	0.63	455	215	0.49	1769	2.6	0.05108	14.7	3.62	0.10	—
2.1.1	1.59	486	282	0.60	1763	2.3	0.05870	11.8	3.60	0.09	—

Grain.area .replicate	$^{206}Pb_c$ (%)	U (ppm)	Th (ppm)	^{232}Th /^{238}U	^{238}U /^{206}Pb	±1σ (%)	^{207}Pb /^{206}Pb	±1σ (%)	Date (Ma)	±1σ (Ma)	Disc (%)
1.1.1	3.76	340	126	0.38	1742	2.4	0.07578	9.7	3.56	0.09	—
13.1.1	-0.06	919	551	0.62	1823	2.2	0.04565	10.3	3.54	0.08	—
4.1.1	0.80	460	276	0.62	1817	1.8	0.05244	13.7	3.52	0.07	—
21.1.1	1.03	417	204	0.51	1830	1.5	0.05423	14.6	3.48	0.06	—
7.1.1	-1.00	663	280	0.44	1868	1.8	0.03823	14.2	3.48	0.07	—
18.1.1	3.39	463	254	0.57	1795	1.3	0.07286	11.9	3.47	0.06	—
22.1.1	1.34	447	194	0.45	1839	1.8	0.05668	14.2	3.46	0.07	—
32.1.1	0.17	464	63	0.14	1861	2.1	0.04748	16.4	3.46	0.08	—
14.1.1	1.97	351	111	0.33	1829	3.5	0.06165	15.8	3.45	0.13	—
11.1.1	1.09	407	148	0.38	1847	2.6	0.05474	33.1	3.45	0.12	—
24.1.1	3.20	254	84	0.34	1809	3.0	0.07139	17.4	3.45	0.12	—
10.1.1	2.82	459	181	0.41	1820	1.8	0.06836	12.1	3.44	0.07	—
17.1.1	0.48	699	345	0.51	1873	1.3	0.04993	11.8	3.42	0.05	—
15.1.1	-0.57	519	182	0.36	1893	2.2	0.04159	15.5	3.42	0.08	—
20.1.1	1.26	289	107	0.38	1861	1.5	0.05609	19.6	3.42	0.07	—
26.1.1	-0.94	346	108	0.32	1914	2.4	0.03868	23.6	3.40	0.09	—
12.1.1	0.66	718	318	0.46	1905	2.1	0.05131	10.8	3.36	0.07	—
23.1.1	0.38	1358	536	0.41	1940	1.8	0.04908	8.2	3.31	0.06	—
31.1.1	2.94	642	268	0.43	1894	2.2	0.06935	11.1	3.30	0.08	—
9.1.1	-0.47	768	254	0.34	1974	2.3	0.04240	12.6	3.28	0.08	—
29.1.1	0.25	415	233	0.58	1994	1.6	0.04810	16.1	3.22	0.06	—
25.1.1	-0.52	493	165	0.35	2027	2.4	0.04202	18.2	3.20	0.08	—
19.1.1	1.46	574	189	0.34	1992	2.2	0.05765	12.3	3.19	0.08	—

2.2. Subvolcanic diorite intruding breccia, Bulolo Volcanics

***Table 2.3** Summary of results: subvolcanic diorite, Bulolo Volcanics (MRA 100214, GA 2131308).*

MRA SiteID	DNM000051
MRA SampleNo	100338
GA SampleNo	2131310
Lithology	Subvolcanic diorite intruding volcanic breccia
Stratigraphic Unit	Bulolo Volcanics
1:250 000 Sheet	WAU (SB55-14)
1:100 000 Sheet	WAU (8283)
WGS84 Location (Geographic)	7.318398°S, 146.626320°E
WGS84 Location (UTM Zone 55)	458755 mE, 9191036 mN
Analytical Session(s)	120071 (see Appendix Table A.1 for parameters derived from measurements of $^{238}U/^{206}Pb$ and $^{207}Pb/^{206}Pb$ reference zircons)
Interpreted Age	3.22 ± 0.06 Ma (95% confidence; 32 analyses of 32 zircons)
Geological Attribution	Magmatic crystallisation
Isotopic Ratio(s) Used	$^{238}U/^{206}Pb$ (^{207}Pb-corrected)

2.2.1. Sampling Details, Rock Description and Geological Relationships

This sample was collected from an aggregate quarry along the Hidden Valley mine access road, about 6.5 km north-northwest of Edie Creek.

The unit sampled for geochronology is a massive, homogeneous, dark grey, plagioclase-phyric diorite, comprising about 10–15% phenocrysts of euhedral plagioclase 1–3 mm in diameter, and about 5% hornblende phenocrysts, set in a fine-grained groundmass. The diorite intrudes a volcanic breccia of the Bulolo Volcanics which also contains fragments of carbonised wood. The contact is steeply dipping and marked by mild shearing, and the dip of the volcanic breccia steepens towards the contact.

The diorite resembles some of the volcanic rocks in the Bulolo Volcanics, and it is interpreted to be a subvolcanic intrusion related to the volcanic rocks. This sample, in conjunction with sample MRA 100214 (GA 2131308), was analysed in an attempt to better constrain the age of the Bulolo Volcanics.

2.2.2. Zircon Description

The mounted crystals are equant to moderately elongate and mostly quite small, with long axes and aspect ratios (length/width) spanning the ranges 20–220 μm and 1–4, respectively (Figure 2.4). Some of the crystal forms are euhedral, but most are subhedral, and grain fragments are common. External morphologies encompass faceted prismatic crystals (with and without pyramidal terminations) and rounded grains. In transmitted light, the crystals are predominantly transparent and colourless to pale pink, and some host inclusions of pale- and dark-coloured minerals (Figure 2.4).

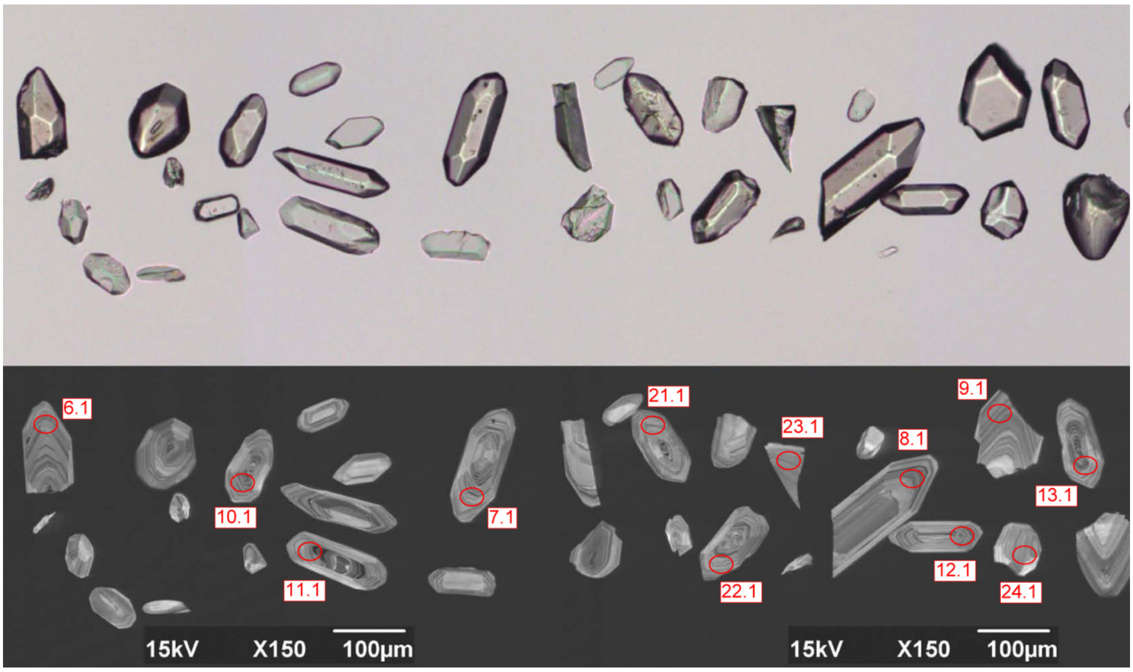

Figure 2.4 *Representative zircons from the subvolcanic diorite, Bulolo Volcanics (MRA 100338, GA 2131310). Transmitted-light image is shown in the upper half; cathodoluminescence image in the lower half. SHRIMP analysis sites are indicated, and labelled with grain and area number.*

Cathodoluminescence (CL) images reveal moderate to high CL emission intensity, and predominantly margin-parallel oscillatory zoning patterns from centre to edge. Discernible core regions are rare, typically characterised by lower CL emission intensity, and are semi-conformably overgrown by brighter-CL zircon with moderate-contrast oscillatory zoning (e.g. grain 11; Figure 2.4). The largely uniform appearance of the zircon population is probably indicative of a single population representing magmatic crystallisation of the host diorite, with little inheritance of antecrystic or xenocrystic cores.

2.2.3. U-Pb Isotopic Results

Thirty-seven analyses were obtained from 37 zircon crystals, and the results are presented in Figures 2.5–2.6 and Table 2.4. Two analyses were characterised by relatively high common Pb ($^{206}Pb_c$ > 7%), so these analyses are interpreted as unreliable, and are not considered further.

The remaining 35 analyses are characterised by a wide range of U (143–1032 ppm, median 315 ppm) and Th/U (0.05–0.91, median 0.60), and mostly low to moderate $^{206}Pb_c$ (maximum 4.85%, median 0.89%). They can be divided into two groups (Table 2.4) based on textural and isotopic criteria:

- Group 1 comprises 32 analyses of 32 zircons, sited within crystals with high CL emission and uniform concentric oscillatory zoning. Their individual ^{207}Pb-corrected $^{238}U/^{206}Pb$ dates range between c. 3.50 Ma and c. 2.91 Ma (Figures 2.5–2.6), and define a weighted mean date of 3.25 ± 0.05 Ma (95% confidence), although the scatter of the constituent analyses exceeds that expected from the individual analytical uncertainties (MSWD = 2.4, P_{equiv} = 0.000).
- Group 2 comprises three analyses of three zircons. One analysis (32.1.1) was sited within a crystal fragment, and one of the other two (11.1.1) sampled high-CL oscillatory zoned zircon but also overlaps an inherited core with markedly lower CL emission (Figure 2.4). Their individual ^{207}Pb-corrected $^{238}U/^{206}Pb$ dates range between c. 50.9 Ma and c. 3.6 Ma (Figures 2.5–2.6).

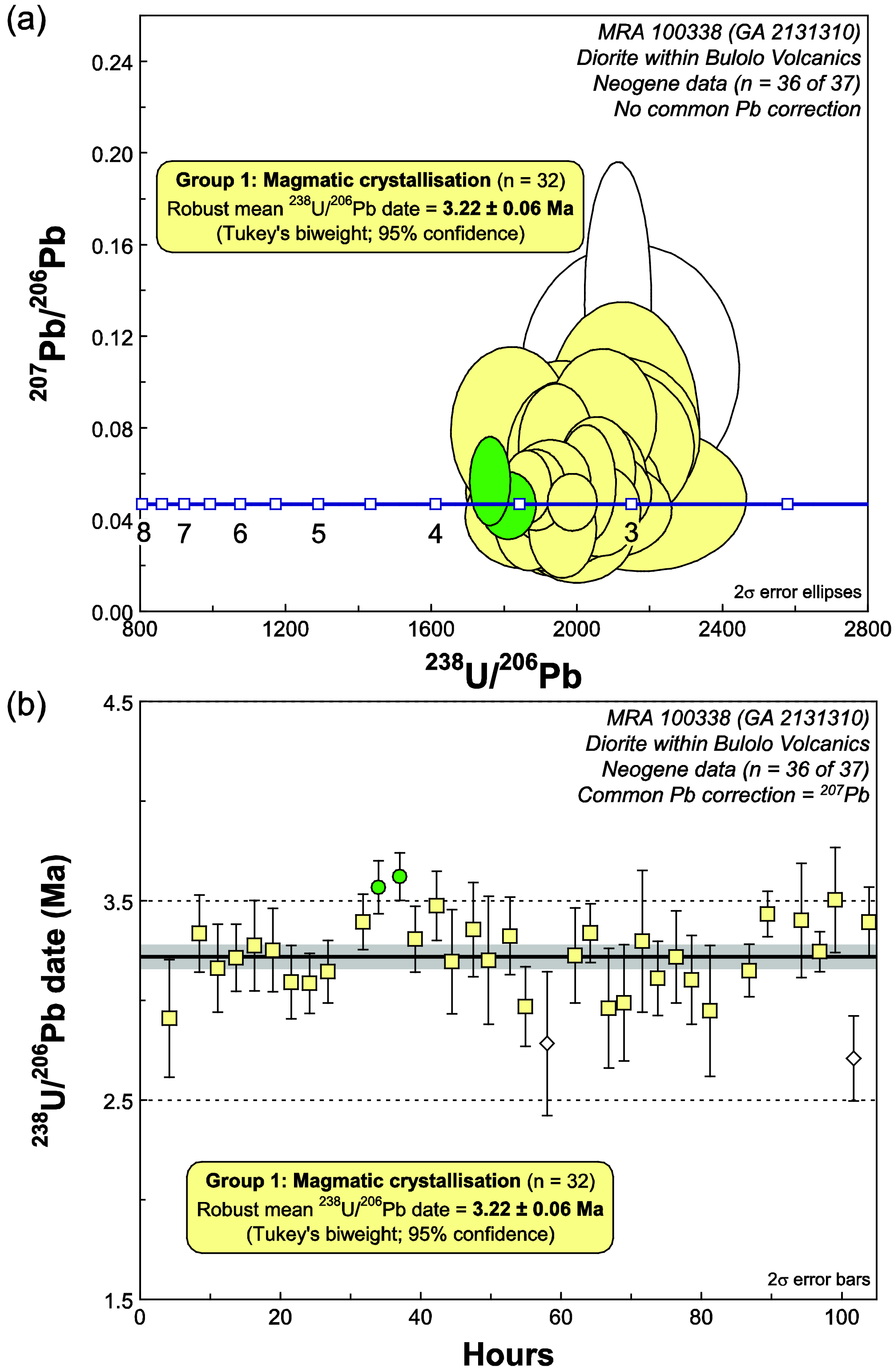

Figure 2.5 *SHRIMP U-Pb data for zircons from the subvolcanic diorite, Bulolo Volcanics (MRA 100338, GA 2131310). (a) Tera-Wasserburg concordia diagram (analysis 32.1.1 not shown); (b) Post-5.0 Ma $^{238}U/^{206}Pb$ dates in order of acquisition. Pale yellow fill denotes Group 1 (magmatic crystallisation); green fill denotes Group 2 (Eocene–Pliocene inheritance); white fill denotes relatively high common Pb ($^{206}Pb_c$ > 7%). Heavy black line and grey band: weighted mean $^{238}U/^{206}Pb$ date and its 95% confidence interval.*

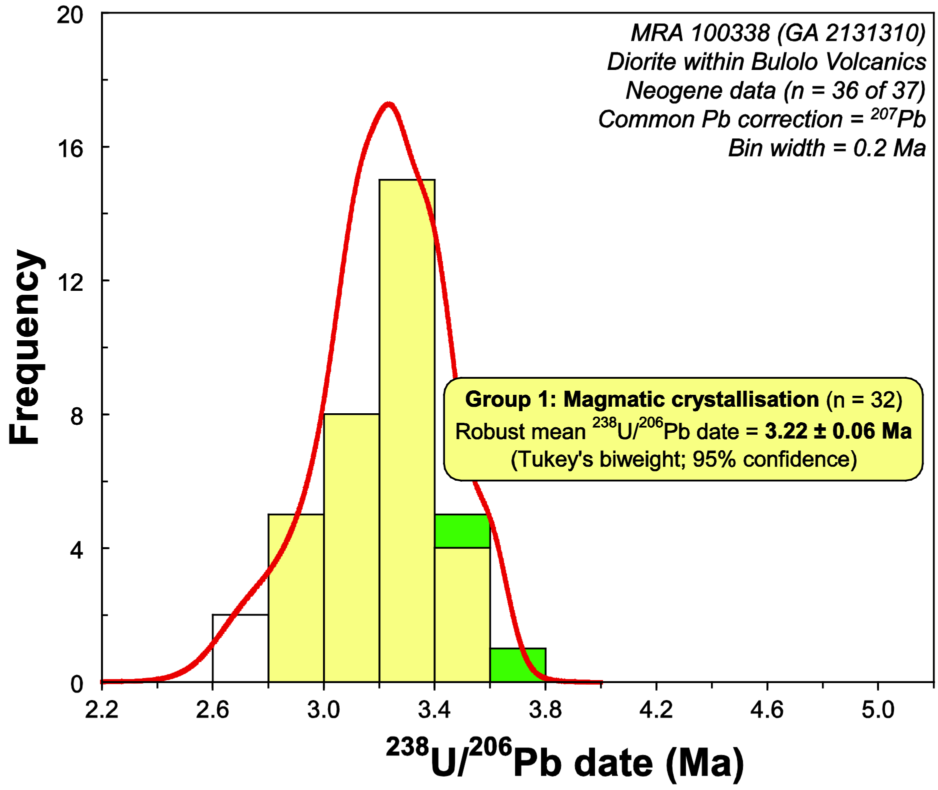

Figure 2.6 *Frequency histogram and probability density distribution for post-5.0 Ma analyses from the subvolcanic diorite, Bulolo Volcanics (MRA 100338, GA 2131310). Pale yellow fill denotes Group 1 (magmatic crystallisation); green fill denotes Group 2 (Eocene–Pliocene inheritance); white fill denotes relatively high common Pb ($^{206}Pb_c$ > 7%). Heavy red curve: relative probability density distribution.*

2.2.4. Geochronological Interpretation

The weighted mean ^{207}Pb-corrected $^{238}U/^{206}Pb$ date of 3.25 ± 0.05 Ma (95% confidence) obtained from the 32 analyses in Group 1 is interpreted as an estimate of the magmatic crystallisation age of the diorite, even though the scatter of the constituent analyses (MSWD = 2.4, P_{equiv} = 0.000) significantly exceeds that expected from the individual analytical uncertainties.

Ordinarily, this would indicate that the statistical coherence of the 32 analyses in Group 1 is compromised by geological sources of variation, such as the inclusion of analyses with individual $^{238}U/^{206}Pb$ dates that are 'pre-magmatic' (e.g. sampling marginally older inherited zircons) and/or 'post-magmatic' (e.g. sampling zircon domains affected by post-crystallisation loss of radiogenic Pb). In this case, however, the probability density distribution (Figure 2.6) is quite symmetrical about its maximum value, and the intrinsically asymmetric 95% confidence interval on the median $^{238}U/^{206}Pb$ date for Group 1 (3.22 +0.09/-0.07 Ma) displays similar symmetry.

These observations suggest that if the observed scatter is truly geological in origin, then analyses of inherited zircon and zircon affected by loss of radiogenic Pb must be present in Group 1 in roughly equal proportions. This seems unlikely, so it is possible that the apparent scatter of the analyses in Group 1 is non-geological. For example, the effect of very low count rates measured by SHRIMP at mass ^{206}Pb in Late Pliocene zircons with only moderate U contents (median c. 7 counts per second for the 32 analyses in Group 1) may have been underestimated by the data-processing software, resulting in individual $^{238}U/^{206}Pb$ analyses being assigned uncertainties that are too small.

Consequently, a mean ^{207}Pb-corrected ^{238}U/^{206}Pb date for Group 1 (Figure 2.6) is most appropriately calculated using the robust Tukey's Biweight method (Hoaglin et al., 1983, implemented by Ludwig, 2009), which ignores the uncertainties assigned to the individual analyses, and instead weights the analyses according to their scatter from an (iteratively-determined) mean.

The resulting robust mean ^{207}Pb-corrected ^{238}U/^{206}Pb date for the 32 analyses in Group 1 is 3.22 ± 0.06 Ma, which is interpreted as the best estimate of the magmatic crystallisation age of the diorite. Based on the field evidence for an intrusive relationship at the sample locality, the robust mean date of 3.22 ± 0.06 Ma also represents a minimum constraint on the eruption age of the host volcanic breccia within the Bulolo Volcanics.

The three analyses in Group 2 are interpreted to have sampled (or at least partly overlapped) 'pre-magmatic' xenocrystic or antecrystic zircons of Eocene to Pliocene age.

Table 2.4 *SHRIMP U-Pb zircon data from the subvolcanic diorite, Bulolo Volcanics (MRA 100338, GA 2131310). Unless otherwise indicated in the Group heading, all isotopic ratios are uncorrected for common Pb and all dates are ^{207}Pb-corrected ^{238}U/^{206}Pb.*

Grain.area .replicate	^{206}Pb$_c$ (%)	U (ppm)	Th (ppm)	^{232}Th /^{238}U	^{238}U /^{206}Pb	±1σ (%)	^{207}Pb /^{206}Pb	±1σ (%)	Date (Ma)	±1σ (Ma)	Disc (%)
Group 2: Eocene–Pliocene inheritance (n = 3)											
32.1.1	0.39	278	151	0.56	126	1.8	0.05014	4.7	50.94	0.92	—
12.1.1	1.35	433	258	0.62	1756	1.3	0.05674	13.9	3.62	0.06	—
11.1.1	-0.01	645	160	0.26	1807	1.7	0.04605	12.9	3.57	0.07	—
Group 1: Magmatic crystallisation (n = 32)											
35.1.1	-0.54	314	75	0.25	1849	3.6	0.04182	22.3	3.50	0.13	—
14.1.1	-0.48	569	210	0.38	1864	2.2	0.04233	23.4	3.47	0.09	—
31.1.1	1.04	603	371	0.64	1857	1.5	0.05433	11.8	3.43	0.06	—
33.1.1	4.21	217	103	0.49	1815	3.7	0.07938	18.6	3.40	0.14	—
10.1.1	0.88	556	298	0.55	1882	1.8	0.05304	13.6	3.39	0.07	—
37.1.1	-0.61	365	165	0.47	1911	2.3	0.04133	23.2	3.39	0.09	—
16.1.1	-0.84	166	96	0.60	1937	3.3	0.03946	24.5	3.36	0.12	—
22.1.1	-1.30	353	179	0.52	1955	1.9	0.03587	24.2	3.34	0.07	—
2.1.1	0.66	392	237	0.62	1919	2.7	0.05132	15.5	3.34	0.10	—
18.1.1	0.07	558	249	0.46	1938	2.8	0.04663	15.2	3.32	0.10	—
13.1.1	1.39	491	235	0.49	1922	2.3	0.05711	12.7	3.31	0.08	—
25.1.1	0.89	155	66	0.44	1937	5.2	0.05314	22.5	3.30	0.18	—
5.1.1	-1.37	335	224	0.69	1995	3.3	0.03530	25.9	3.28	0.11	—
6.1.1	-0.08	269	180	0.69	1983	2.9	0.04547	22.1	3.25	0.10	—
34.1.1	0.19	1032	49	0.05	1982	1.4	0.04761	10.7	3.24	0.05	—
21.1.1	1.68	221	106	0.49	1965	3.2	0.05941	24.0	3.23	0.12	—
27.1.1	2.54	212	113	0.55	1952	3.1	0.06616	21.1	3.22	0.12	—

Grain.area .replicate	$^{206}Pb_c$ (%)	U (ppm)	Th (ppm)	$^{232}Th/^{238}U$	$^{238}U/^{206}Pb$	±1σ (%)	$^{207}Pb/^{206}Pb$	±1σ (%)	Date (Ma)	±1σ (Ma)	Disc (%)
4.1.1	3.33	272	162	0.62	1938	2.2	0.07239	15.3	3.21	0.08	—
17.1.1	1.11	307	210	0.70	1991	4.8	0.05486	19.5	3.20	0.16	—
15.1.1	3.23	187	105	0.58	1952	3.6	0.07161	21.7	3.19	0.13	—
3.1.1	1.63	315	230	0.76	2005	3.2	0.05901	17.5	3.16	0.11	—
30.1.1	1.21	358	279	0.80	2022	1.6	0.05569	18.8	3.15	0.07	—
9.1.1	-0.28	257	177	0.71	2055	2.3	0.04393	18.4	3.14	0.08	—
26.1.1	0.72	453	401	0.91	2057	2.8	0.05177	15.0	3.11	0.09	—
28.1.1	-0.18	410	323	0.81	2081	3.4	0.04472	19.0	3.10	0.11	—
7.1.1	1.48	343	250	0.75	2054	2.7	0.05781	17.6	3.09	0.09	—
8.1.1	1.93	374	249	0.69	2048	2.1	0.06137	15.7	3.09	0.08	—
24.1.1	3.28	203	126	0.64	2086	4.5	0.07198	19.9	2.99	0.15	—
19.1.1	4.85	274	171	0.64	2066	2.9	0.08436	14.7	2.97	0.10	—
23.1.1	3.85	163	81	0.51	2093	4.7	0.07648	18.8	2.96	0.15	—
29.1.1	0.42	143	61	0.44	2178	5.3	0.04945	26.0	2.95	0.16	—
1.1.1	4.38	281	205	0.75	2118	4.1	0.08066	27.7	2.91	0.15	—
Not considered: $^{206}Pb_c$ > 7% (n = 2)											
20.1.1	7.51	126	70	0.58	2141	5.7	0.10541	21.4	2.78	0.18	—
36.1.1	11.41	155	73	0.49	2108	1.8	0.13619	18.0	2.71	0.11	—

3. Morobe Granodiorite

The Morobe Granodiorite forms two batholiths (with exposure area exceeding 600 km^2) in the Kuper and Ekuti Ranges, as well as a number of smaller intrusions in the Wau–Bulolo area. The granodiorite intrudes the Owen Stanley Metamorphics (although it postdates thrusting and metamorphism in the latter unit), and is overlain nonconformably by the Pliocene Bulolo Volcanics and Otibanda Formation.

Previous K-Ar dating of the small granodiorite masses along Watut River northwest of Bulolo yielded middle Miocene dates of c. 14 Ma (from hornblende) and c. 13 Ma (from biotite), whereas the main masses in the Ekuti and Kuper Ranges yielded marginally younger K-Ar dates of c. 12 Ma from hornblende, and c. 11 Ma from biotite (Page, 1976). Four hornblende K-Ar determinations by Cussen et al. (1986) yielded dates ranging from 15.1 ± 0.2 Ma to 12.0 ± 0.1 Ma. In addition, three biotite Rb-Sr analyses indicate middle Miocene dates between c. 14.5 Ma and c. 12.7 Ma (Page, 1976).

3.1. Morobe Granodiorite

***Table 3.1** Summary of results: Morobe Granodiorite (MRA 100417, GA 2131311).*

MRA SiteID	ALB000035
MRA SampleNo	100417
GA SampleNo	2131311
Lithology	Massive biotite-hornblende granodiorite
Stratigraphic Unit	Morobe Granodiorite
1:250 000 Sheet	WAU (SB55-14)
1:100 000 Sheet	WAU (8283)
WGS84 Location (Geographic)	7.088590°S, 146.635718°E
WGS84 Location (UTM Zone 55)	459772 mE, 9216442 mN
Analytical Session(s)	120071 (see Appendix Table A.1 for parameters derived from measurements of $^{238}U/^{206}Pb$ and $^{207}Pb/^{206}Pb$ reference zircons)
Interpreted Age	13.62 ± 0.13 Ma (95% confidence; 27 analyses of 27 zircons)
Geological Attribution	Magmatic crystallisation
Isotopic Ratio(s) Used	$^{238}U/^{206}Pb$ (^{207}Pb-corrected)

3.1.1. Sampling Details, Rock Description and Geological Relationships

This sample was collected from an exposure in a road cutting along the Upper Baiune road, about 4 km east-southeast of Sam Sam No 1 village.

The Morobe Granodiorite is dominated by medium-grained biotite-hornblende granodiorite hosting abundant mafic inclusions. Round inclusions of diorite are widespread, contain plagioclase phenocrysts that resemble those in the host granodiorite, and preserve textures interpreted to reflect mafic–felsic magma mingling (Saroa et al., 2012). One net-vein complex, indicative of magma mingling, was also identified along the Watut Road near Paroa village. Subangular to subrounded inclusions of hornfelsed phyllite (with biotite porphyroblasts) are less common in the Morobe Granodiorite, and subrounded, chlorite-rich inclusions of mafic or ultramafic origin are relatively rare.

The unit sampled for geochronology is a massive, equigranular biotite-hornblende granodiorite which will better constrain the igneous crystallisation age of the Morobe Granodiorite.

3.1.2. Zircon Description

The mounted crystals are equant to moderately elongate, with long axes and aspect ratios (length/width) spanning the ranges 40–220 μm and 1–5, respectively (Figure 3.1). Crystal forms are euhedral to subhedral, and external morphologies dominated by faceted prismatic grains with well-developed pyramidal terminations. In transmitted light, the crystals are predominantly transparent, colourless to pale pink, and many host very fine-grained inclusions of dark-coloured minerals (Figure 3.1). No obviously inherited cores are visible in transmitted light.

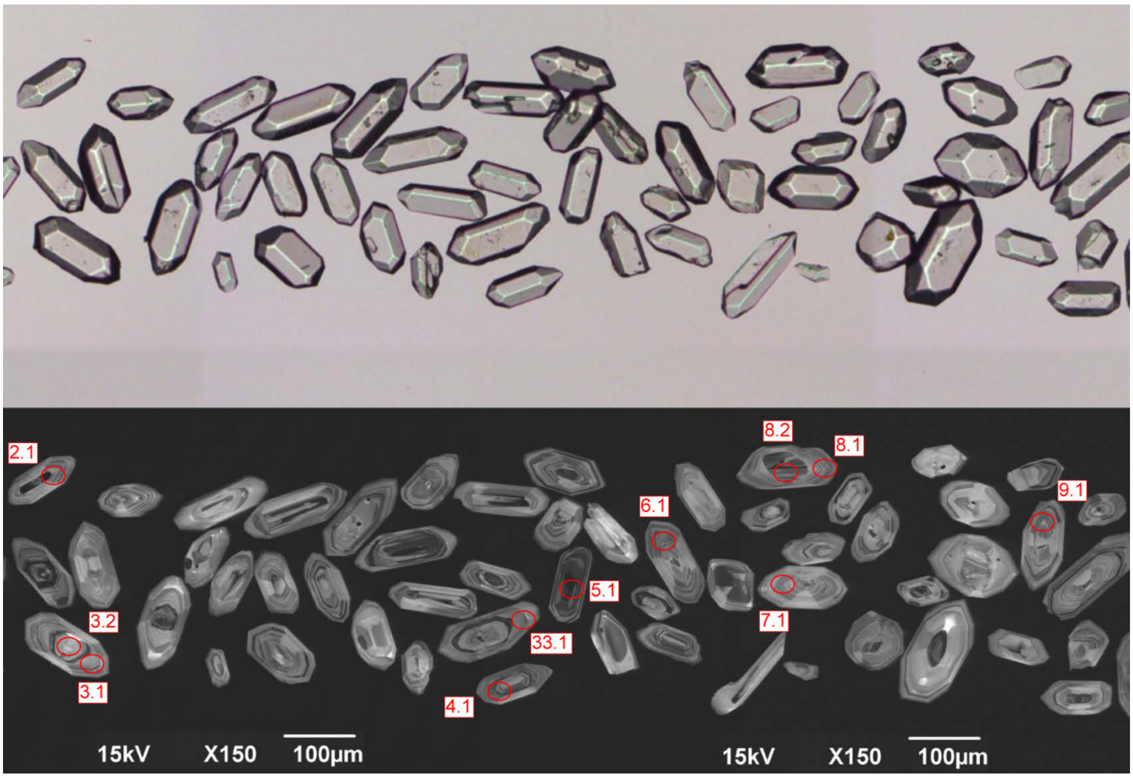

Figure 3.1 *Representative zircons from the Morobe Granodiorite (MRA 100417, GA 2131311). Transmitted-light image is shown in the upper half; cathodoluminescence image in the lower half. SHRIMP analysis sites are indicated, and labelled with grain and area number.*

Cathodoluminescence (CL) images reveal moderate to high CL emission intensities, and predominantly margin-parallel oscillatory zoning patterns. Up to half of all the mounted crystals are characterised by the presence of core regions with relatively indistinct zoning patterns and CL emission intensities which vary widely from grain to grain. Zoning in the cores is invariably truncated by disconformable pyramidal terminations, with uniformly high CL emission and moderate-contrast oscillatory zoning (Figure 3.1). The uniform appearance of the pyramidal overgrowths means it is likely that they represent magmatic crystallisation of the host granodiorite, with the heterogeneous core regions reflecting a variety of older zircons inherited by the magma.

3.1.3. U-Pb Isotopic Results

Thirty-seven analyses were obtained from 33 zircon crystals, and the results are presented in Figures 3.2–3.3 and Table 3.2. Four grains (3, 8, 10 and 13) were each analysed twice. One analysis is characterised by relatively high common Pb ($^{206}Pb_c$ > 4%), and two others are unsatisfactorily sited so that they overlap core and rim zircon domains with markedly different CL emission characteristics. These three analyses are interpreted as unreliable, and are not considered further.

The remaining 34 analyses are characterised by predominantly low to moderate U contents (145–2153 ppm, median 247 ppm), moderate Th/U (0.38–1.19, median 0.71), and mostly low $^{206}Pb_c$ (maximum 1.72%, median 0.05%). They can be divided into three groups (Table 3.2) based on chemical, textural and isotopic criteria:

- Group 1 comprises 27 analyses of 27 zircons with uniformly low to moderate U (147–401 ppm, median 242 ppm) and moderate to high Th/U (0.57–1.19, median 0.77). The analyses are sited within the outer parts of crystals, and are characterised by high CL emission and margin-parallel oscillatory zoning. Their individual ^{207}Pb-corrected $^{238}U/^{206}Pb$ dates range between c. 14.28 Ma and c. 13.07 Ma (Figures 3.2–3.3), and define a weighted mean date of 13.62 ± 0.13 Ma (95% confidence; MSWD = 1.32, P_{equiv} = 0.13).
- Group 2 comprises a single analysis, sited in the outer part of a crystal with high CL emission and margin-parallel oscillatory zoning, similar to those in Group 1. Its U content (227 ppm) and Th/U (0.72) are also similar to those in Group 1, but its individual ^{207}Pb-corrected $^{238}U/^{206}Pb$ date of 14.66 ± 0.61 Ma (2σ) is slightly older than those in Group 1 (Figures 3.2–3.3).
- Group 3 comprises six analyses of six zircons. Four are sited within core regions with low to moderate CL emission, and are disconformably overgrown by high-CL oscillatory-zoned zircon, analyses of which lie within Group 1 in each case. The six analyses encompass a wide range of U contents (145–2153 ppm, median 626 ppm), but are characterised by moderate Th/U (0.39–0.91, median 0.56). Their individual ^{204}Pb-corrected $^{238}U/^{206}Pb$ dates range between c. 397 Ma and c. 182 Ma (Figure 3.2), with the youngest two clustered at 186.7 ± 4.1 Ma (2σ, MSWD = 1.9, P_{equiv} = 0.17), and three of the remaining four clustered at 233.9 ± 4.0 Ma (2σ, MSWD = 0.23, P_{equiv} = 0.80).

3.1.4. Geochronological Interpretation

The weighted mean ^{207}Pb-corrected $^{238}U/^{206}Pb$ date of 13.62 ± 0.13 Ma (95% confidence) obtained from the 27 analyses in Group 1 is interpreted as the best estimate of the magmatic crystallisation age of the Morobe Granodiorite.

The single analysis in Group 2 is interpreted as a ‘pre-magmatic’ xenocrystic zircon of Miocene age, and the six analyses in Group 3 are interpreted as xenocrysts and inherited cores of Devonian–Cretaceous age, which have been entrained in the Morobe Granodiorite magma.

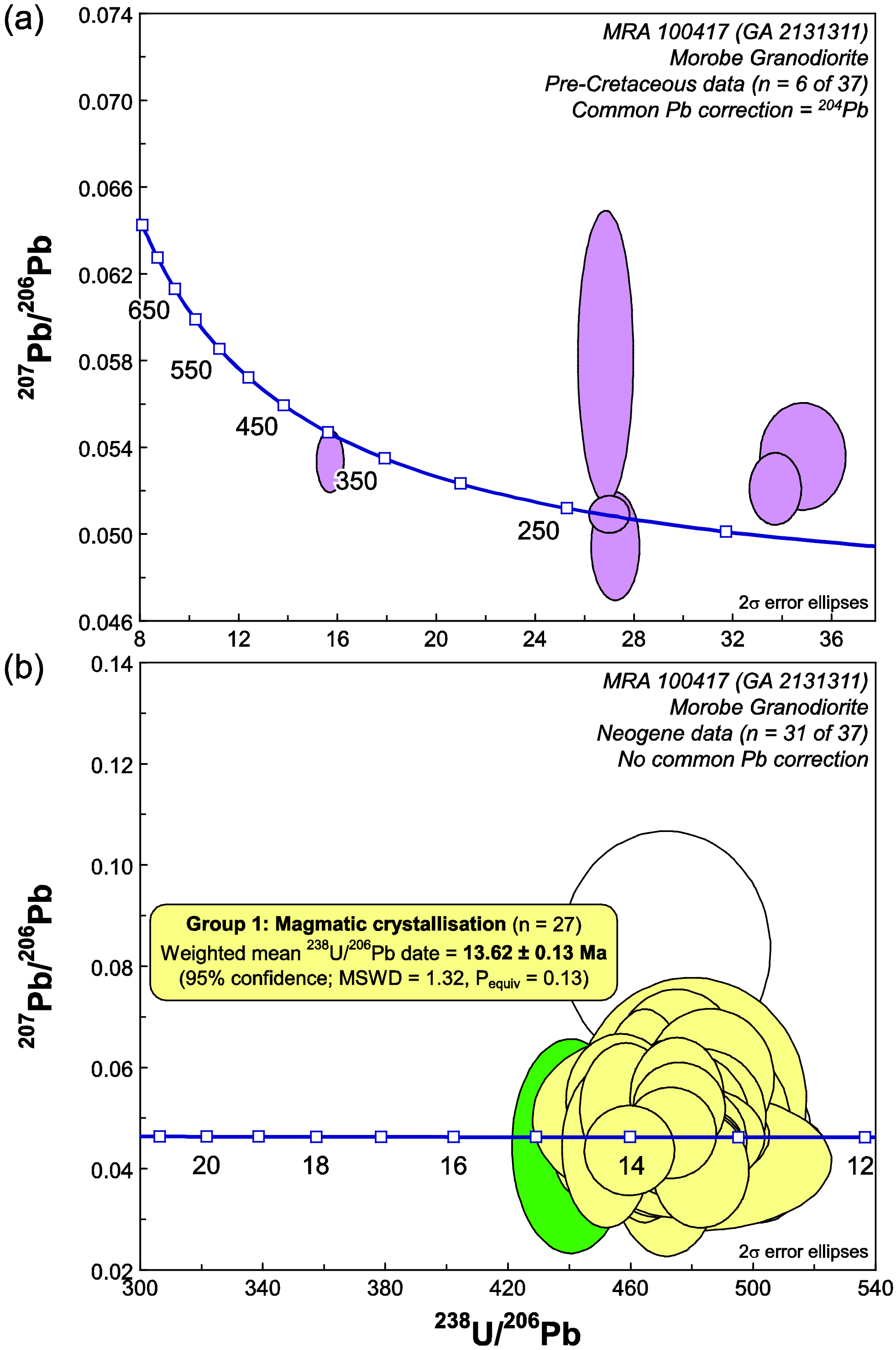

Figure 3.2 *Tera-Wasserburg concordia diagrams for SHRIMP U-Pb zircon data from the Morobe Granodiorite (MRA 100417, GA 2131311). (a) Pre-Cretaceous data; (b) Neogene data. Pale yellow fill denotes Group 1 (magmatic crystallisation); green fill denotes Group 2 (Miocene inheritance); pink fill denotes Group 3 (pre-Cretaceous inheritance); white fill denotes analyses not considered ($^{206}Pb_c$ > 4%, or affected by core-rim overlap).*

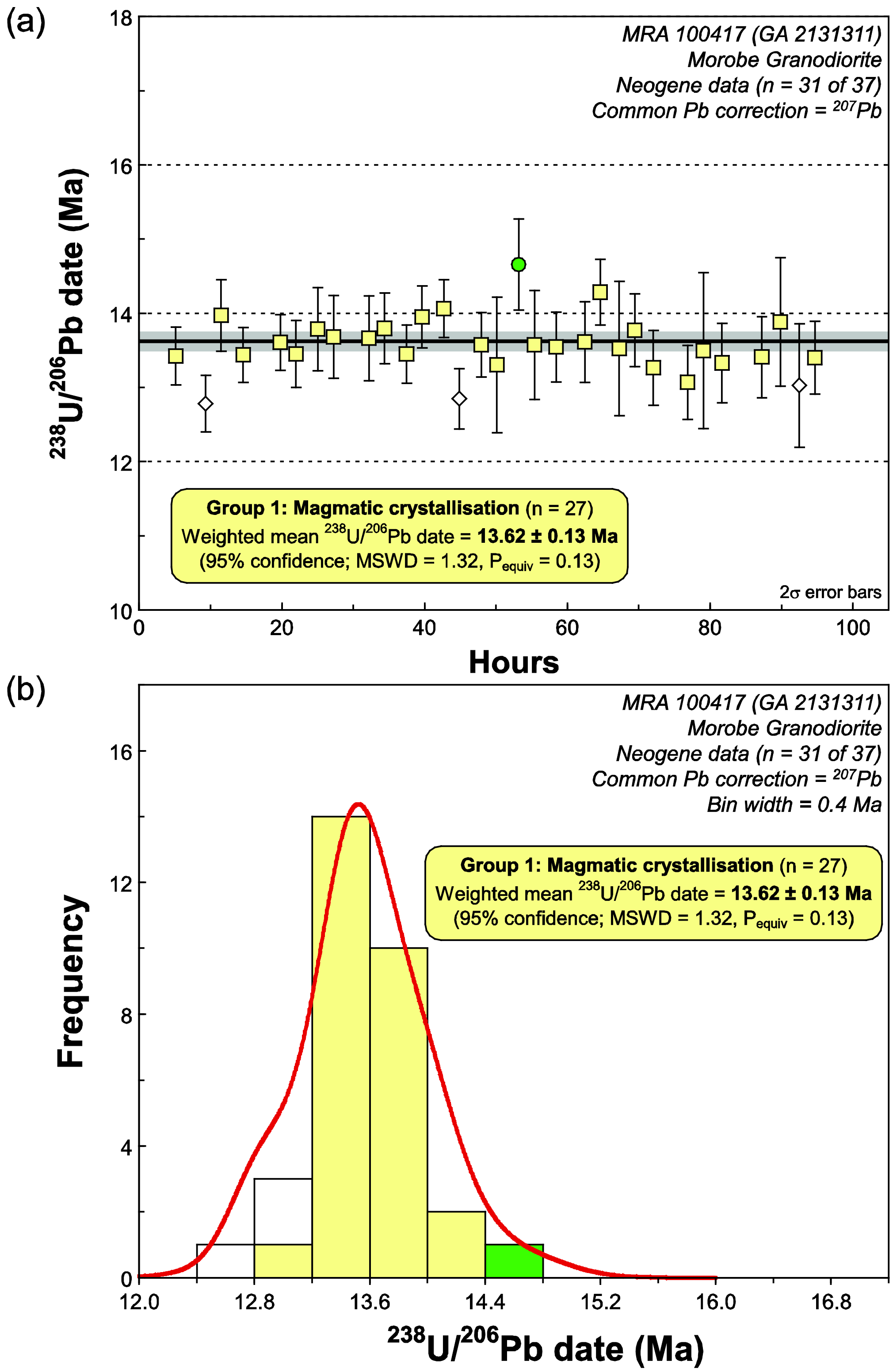

Figure 3.3 *Neogene analyses from the Morobe Granodiorite (MRA 100417, GA 2131311). (a) Individual $^{238}U/^{206}Pb$ dates in order of acquisition; (b) Frequency histogram and probability density distribution. Pale yellow fill denotes Group 1 (magmatic crystallisation); green fill denotes Group 2 (Miocene inheritance); pink fill denotes Group 3 (pre-Cretaceous inheritance); white fill denotes analyses not considered ($^{206}Pb_c$ > 4%, or affected by core-rim overlap). Heavy black line and grey band: weighted mean $^{238}U/^{206}Pb$ date and its 95% confidence interval; heavy red curve: relative probability density distribution.*

Table 3.2 *SHRIMP U-Pb zircon data from the Morobe Granodiorite (MRA 100417, GA 2131311). Unless otherwise indicated in the Group heading, all isotopic ratios are uncorrected for common Pb and all dates are* ^{207}*Pb-corrected* ^{238}*U/*^{206}*Pb.*

Grain.area .replicate	$^{206}Pb_c$ (%)	U (ppm)	Th (ppm)	$^{232}Th/^{238}U$	$^{238}U/^{206}Pb$	±1σ (%)	$^{207}Pb/^{206}Pb$	±1σ (%)	Date (Ma)	±1σ (Ma)	Disc (%)
Group 3: Pre-Cretaceous inheritance (n = 6; isotopic ratios, dates and discordance are ^{204}Pb-corrected)											
8.2.1	-0.18	633	346	0.56	15.75	1.44	0.05338	1.1	396.7	5.5	-16
3.2.1	-0.06	145	128	0.91	26.86	1.71	0.05820	4.7	235.7	4.0	57
5.1.1	0.04	2153	807	0.39	27.03	1.25	0.05096	0.7	234.2	2.9	2
26.1.1	-0.26	357	190	0.55	27.26	1.46	0.04949	2.0	232.3	3.3	-36
10.2.1	0.25	914	474	0.54	33.72	1.27	0.05214	1.3	188.4	2.4	36
13.2.1	0.61	618	416	0.70	34.84	2.04	0.05362	1.9	182.4	3.7	49
Group 2: Miocene inheritance (n = 1)											
18.1.1	-0.21	227	159	0.72	440.3	1.8	0.04470	19.3	14.66	0.31	—
Group 1: Magmatic crystallisation (n = 27)											
22.1.1	-0.23	379	436	1.19	451.9	1.3	0.04447	14.5	14.28	0.22	—
14.1.1	-0.31	354	290	0.85	459.4	1.3	0.04387	8.2	14.06	0.19	—
3.1.1	0.96	193	170	0.91	456.5	1.6	0.05389	9.8	13.97	0.24	—
13.1.1	0.75	205	137	0.69	458.2	1.3	0.05226	10.0	13.95	0.21	—
31.1.1	0.49	190	111	0.61	461.5	3.0	0.05019	13.1	13.88	0.43	—
11.1.1	0.55	214	129	0.62	464.2	1.3	0.05066	16.9	13.80	0.24	—
8.1.1	0.28	286	224	0.81	465.8	2.0	0.04853	9.0	13.78	0.28	—
24.1.1	-0.12	180	107	0.61	468.2	1.6	0.04539	13.2	13.77	0.25	—
9.1.1	-0.72	267	184	0.71	474.1	2.0	0.04065	10.0	13.68	0.28	—
10.1.1	-0.04	204	141	0.71	471.6	1.7	0.04601	20.5	13.66	0.29	—
21.1.1	-0.13	401	296	0.76	473.7	2.0	0.04526	7.7	13.61	0.27	—
6.1.1	0.13	394	338	0.89	472.7	1.3	0.04734	7.8	13.61	0.19	—
16.1.1	0.54	147	158	1.11	471.8	1.4	0.05059	12.1	13.57	0.22	—
19.1.1	0.06	278	245	0.91	474.2	2.7	0.04681	8.8	13.57	0.37	—
20.1.1	-0.35	355	265	0.77	477.2	1.7	0.04353	8.8	13.54	0.24	—
23.1.1	0.32	219	164	0.77	474.7	3.2	0.04882	16.8	13.52	0.45	—
28.1.1	-0.58	198	109	0.57	479.9	3.8	0.04174	13.5	13.50	0.53	—
7.1.1	-0.06	251	230	0.95	479.1	1.6	0.04585	9.9	13.45	0.23	—
12.1.1	-0.79	245	157	0.66	482.6	1.3	0.04007	11.6	13.45	0.20	—
4.1.1	0.74	385	293	0.79	475.6	1.3	0.05218	7.1	13.44	0.19	—
1.1.1	1.01	250	228	0.94	474.8	1.3	0.05426	8.9	13.43	0.19	—
30.1.1	0.02	364	317	0.90	480.2	2.0	0.04649	8.7	13.41	0.27	—
33.1.1	0.32	188	111	0.61	479.0	1.7	0.04881	11.8	13.40	0.24	—
29.1.1	1.72	208	131	0.65	474.8	1.8	0.05993	10.7	13.33	0.27	—

Grain.area .replicate	$^{206}Pb_c$ (%)	U (ppm)	Th (ppm)	$^{232}Th/^{238}U$	$^{238}U/^{206}Pb$	±1σ (%)	$^{207}Pb/^{206}Pb$	±1σ (%)	Date (Ma)	±1σ (Ma)	Disc (%)
17.1.1	0.93	205	121	0.61	479.6	3.2	0.05366	18.5	13.30	0.46	—
25.1.1	0.52	219	148	0.70	483.0	1.8	0.05038	10.9	13.27	0.25	—
27.1.1	1.50	242	208	0.89	485.4	1.8	0.05814	9.6	13.07	0.25	—
Not considered: Affected by core-rim overlap (n = 2)											
15.1.1	-0.16	173	95	0.57	502.1	1.4	0.04503	14.0	12.85	0.20	—
2.1.1	-0.28	522	194	0.38	505.3	1.4	0.04407	6.8	12.78	0.19	—
Not considered: $^{206}Pb_c$ > 4% (n = 1)											
32.1.1	4.70	118	57	0.50	471.2	2.9	0.08340	11.5	13.03	0.42	—

4. Owen Stanley Metamorphics

The Owen Stanley Metamorphics outcrop over a large part of the Papuan Peninsula, structurally beneath the ophiolite of the Papuan Ultramafic Belt, from which it is separated by the Owen Stanley Fault. The most common rock type within the Owen Stanley Metamorphics in the Wau 1:100 000 map sheet is a dark blue-grey phyllite, which contains some lenses or interbeds of foliated metasandstone, metabasalt and calc-silicate rock. The Owen Stanley Metamorphics has been subdivided in the Wau region on the basis of lithology (e.g. Cussen et al., 1986), but these subdivisions do not take into account the likely structural complexity of the unit. The age of the protoliths of the Owen Stanley Metamorphics is not well established, nor are there any published data on their detrital provenance. Macrofossils within low-grade metasedimentary rocks in the northwestern part of the metamorphic complex are Aptian–Cenomanian (Dow et al., 1974) indicating a Cretaceous age for parts of the unit. The supracrustal protoliths of the metamorphics are thought to have been deposited on the passive margin of the Australian Craton, before being thrust-stacked and metamorphosed at low grade during obduction of the Papuan Ultramafic Belt.

Two samples of the Owen Stanley Metamorphics (MRA 100211 and MRA 100215) were targeted for U-Pb SHRIMP detrital zircon analysis. The former is described and documented below; the latter is a foliated metasandstone forming small blocky exposures along a creek bank (WGS84 UTM Zone 55, 465869 mE, 9189116 mN) beside the Kaisenik–Elaru road about 2 km north-northeast of Elaru village. Unfortunately, that sample yielded no zircon, and it is not discussed further.

4.1. Owen Stanley Metamorphics

Table 4.1 *Summary of results: Owen Stanley Metamorphics (MRA 100211, GA 2131307).*

MRA SiteID	CUT000040
MRA SampleNo	100211
GA SampleNo	2131307
Lithology	Foliated metasandstone
Stratigraphic Unit	Owen Stanley Metamorphics
1:250 000 Sheet	WAU (SB55-14)
1:100 000 Sheet	WAU (8283)
WGS84 Location (Geographic)	7.335814°S, 146.690760°E
WGS84 Location (UTM Zone 55)	465869 mE, 9189116 mN
Analytical Session(s)	120088 (see Appendix Table A.1 for parameters derived from measurements of $^{238}U/^{206}Pb$ and $^{207}Pb/^{206}Pb$ reference zircons)
Interpreted Age	282.6 +1.7/-1.3 Ma (95% confidence; 65 analyses of 65 zircons)
Geological Attribution	Maximum age for deposition of the precursor sandstone
Isotopic Ratio(s) Used	$^{238}U/^{206}Pb$ (^{204}Pb-corrected)

4.1.1. Sampling Details, Rock Description and Geological Relationships

This sample was collected from an exposure in a road cutting along the Wau–Mt Kaindi road, about 3 km west-northwest of Wau.

The unit sampled for geochronology is a 1.0–1.5 metre-thick bed of blocky, foliated fine- to medium-grained metasandstone with abundant chlorite and muscovite, within a succession dominated by dark blue-grey phyllite. The sample comprises 10–15% grains about 0.5 mm in diameter (mostly strained quartz, with lesser sericitised plagioclase), in a matrix of anhedral granular quartz, plagioclase, pale orange-brown biotite, muscovite and opaque minerals less than 0.05 mm in diameter. Scattered grains of anhedral to subhedral zircon are evident. A weak schistosity is defined by seams of muscovite and biotite, some of which are crenulated.

Detrital zircons from four samples of 'metagreywacke' from the Owen Stanley Metamorphics have previously been targeted for U-Pb SHRIMP analysis, and documented in an unpublished manuscript by G. Kopi, R.H. Findlay and I.S. Williams. Those samples were collected from three localities: about 15 km southeast, 20 km west-northwest, and 25 km north-northwest of the township of Wau. The current sample will improve the geographical coverage of detrital zircon age data for the Owen Stanley Metamorphics, and provide a more representative indication of the overall provenance of the unit.

4.1.2. Zircon Description

The mounted crystals encompass a range of shapes and sizes, with long axes and aspect ratios (length/width) spanning the ranges 30–320 μm and 1–4, respectively (Figure 4.1). Crystal forms range from euhedral to anhedral, with external morphologies spanning faceted grains with pyramidal terminations, moderately elongate rectangular prismatic crystals, and rounded anhedral grains with frosted and pitted surfaces commonly indicative of prolonged sedimentary transport. In transmitted light, the crystals range from colourless to pale pink, pale yellow, and pale brown, and from transparent to translucent and mottled. Many grains exhibit transverse or longitudinal cracking, and some crystals contain abundant inclusions of pale- or dark-coloured minerals, whereas others are inclusion-free (Figure 4.1). In rare cases, a contrast is evident in transmitted light between an older, mostly inclusion-rich core region and a younger, largely inclusion-free overgrowth.

Cathodoluminescence (CL) images reveal a wide range of CL emission intensities and zoning patterns (Figure 4.1). Most of the faceted grains are dominated by high CL emission and either low-contrast concentric oscillatory zoning or radial sector zoning from centre to edge. In some cases, these zoning patterns are restricted to central domains disconformably overgrown by external mantles or rims of zircon with high CL emission but little internal zoning structure, and several of these proved wide enough for SHRIMP analysis (Figure 4.1). Elongate prismatic crystals are also oscillatory-zoned, but equally commonly exhibit broad, ill-defined and low-contrast banding parallel to their long axes. Many of the anhedral and rounded grains are characterised by uniform CL emission and little development (or preservation) of internal zoning structure. Several crystals display convoluted and chaotic CL zoning, usually corresponding to cracked grains with a mottled appearance in transmitted light (Figure 4.1). The diversity of this zircon population suggests that it was derived from source regions spanning a range of ages and chemical affinities, and the rounded shapes indicate that at least some of the zircons have undergone sedimentary transport in a high-energy depositional environment. This could have occurred during deposition of the sedimentary precursors to the Owen Stanley Metamorphics, or during a previous sedimentation event in the source region, if some of these detrital zircons are polycyclic.

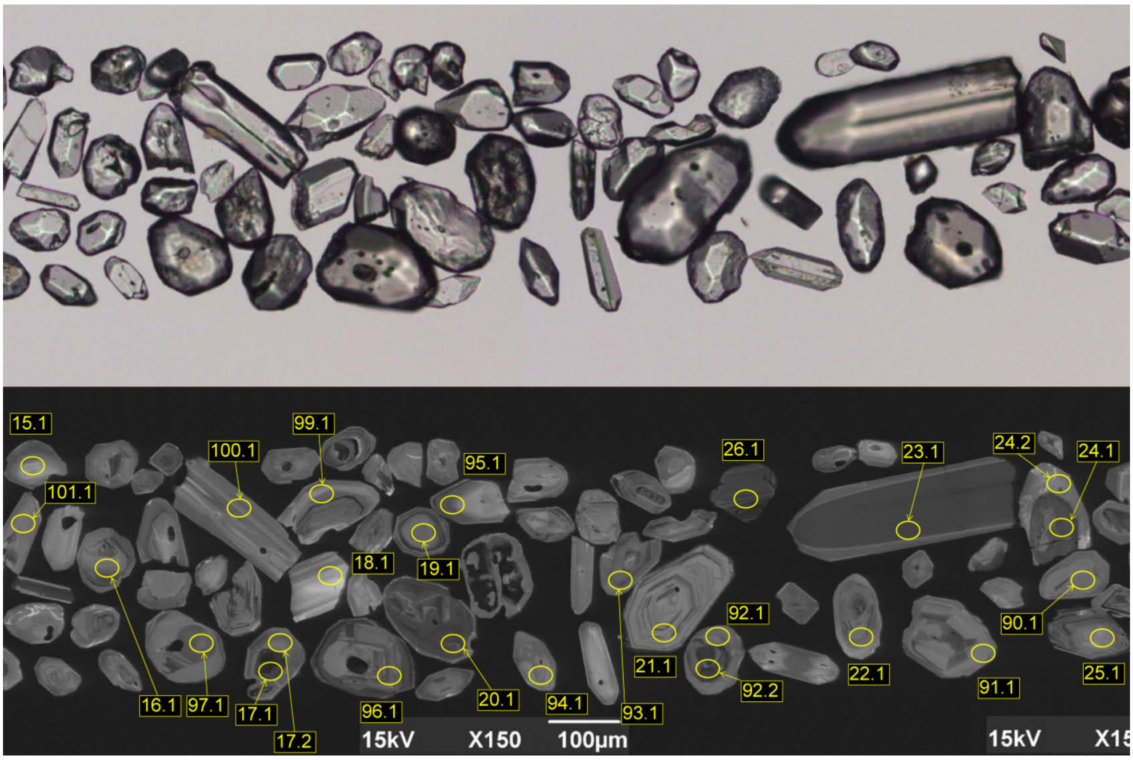

***Figure 4.1** Representative zircons from the Owen Stanley Metamorphics (MRA 100211, GA 2131307). Transmitted-light image is shown in the upper half; cathodoluminescence image in the lower half. SHRIMP analysis sites are indicated, and labelled with grain and area number.*

4.1.3. U-Pb Isotopic Results

One hundred and fifteen analyses were obtained from 111 zircon crystals, and the results are presented in Figures 4.2–4.3 and Table 4.2. Four grains (9, 17, 24 and 92) were each analysed twice. Four analyses yielded large negative values for common Pb ($^{206}Pb_c$ < -1%), which are interpreted to reflect inaccurate common Pb corrections. Another four analyses were characterised by relatively high common Pb ($^{206}Pb_c$ > 1%), and a further three yielded individual ^{204}Pb-corrected $^{207}Pb/^{206}Pb$ dates that are older than 1200 Ma, but more than 10% discordant. These 11 analyses are interpreted as unreliable, and are not considered further.

The remaining 104 analyses are characterised by mostly low to moderate U contents (18–1982 ppm, median 196 ppm), a wide range of Th/U (0.08–1.93, median 0.58), and predominantly low $^{206}Pb_c$ (maximum 0.90%, median 0.01%). They can be divided into four groups (Table 4.2) based on chemical, textural and isotopic criteria:

- Group 1 comprises a single analysis, sited in the centre of a rectangular prismatic zircon with a transverse crack, moderate CL emission and little internal zoning. Its low U content (76 ppm) and moderate Th/U (0.57) resemble those of Group 2 (below), but its individual ^{204}Pb-corrected $^{238}U/^{206}Pb$ date of 247.6 ± 5.2 Ma (2σ) is younger than those in Group 2 (Figures 4.2–4.3).
- Group 2 comprises 65 analyses of 65 zircons, spanning: (i) faceted grains with high CL emission and either low-contrast concentric oscillatory zoning from centre to edge or radial sector zoning, (ii) elongate prismatic crystals with oscillatory zoning or low-contrast, ill-defined banding parallel to their long axes, and (iii) external rims with high CL emission but little internal structure, which disconformably overgrow cores with lower CL emission (Figure 4.1). Analyses

of the cores lie within Groups 3 and 4. Group 2 analyses are characterised by varied but mostly low U contents (18–836 ppm, median 154 ppm), and varied but mostly moderate Th/U (0.09–1.56, median 0.68). Their individual ^{204}Pb-corrected ^{238}U/^{206}Pb dates range between c. 299 Ma and c. 266 Ma, and define a weighted mean date of 283.1 ± 1.2 Ma (95% confidence), although the scatter of the constituent analyses exceeds that expected from the individual analytical uncertainties (MSWD = 3.4, P_{equiv} = 0.000).

- Group 3 comprises 29 analyses of 29 zircons, primarily within subhedral to anhedral crystals with low-contrast oscillatory zoning and CL emission mostly lower than those in Group 2. Some darker-CL cores are disconformably overgrown by brighter-CL zircon rims (Figure 4.1), analyses of which lie within Group 2. Group 3 analyses are characterised by varied but mostly low U contents (33–1982 ppm, median 236 ppm), varied but mostly moderate Th/U (0.15–1.93, median 0.48), and ^{204}Pb-corrected ^{238}U/^{206}Pb dates ranging between c. 1200 Ma and c. 310 Ma.
- Group 4 comprises nine analyses of nine zircons, mostly within subhedral to anhedral crystals with similar CL emission intensities and zoning patterns to those in Group 3. Four have low to moderate U (114–358 ppm, median 241 ppm), moderate Th/U (0.49–0.63, median 0.53), and individual ^{204}Pb-corrected ^{207}Pb/^{206}Pb dates between c. 2804 Ma and c. 1731 Ma. The remaining five have higher U (198–1137 ppm, median 537 ppm), lower Th/U (0.08–0.78, median 0.29), and a more restricted range of individual ^{204}Pb-corrected ^{207}Pb/^{206}Pb dates (c. 1593 Ma to c. 1539 Ma). These five analyses define a statistically coherent weighted mean date of 1551 ± 12 Ma (95% confidence; MSWD = 0.84, P_{equiv} = 0.50).

4.1.4. Geochronological Interpretation

The individual ^{204}Pb-corrected ^{238}U/^{206}Pb date of 247.6 ± 5.2 Ma (2σ) obtained from the single analysis in Group 1 may be interpreted as a maximum estimate for the depositional age of the sedimentary protolith of the metasandstone, as this date does not violate any of the independent geological constraints on the age of the protoliths of the Owen Stanley Metamorphics. However, this date is statistically isolated on the 'young' side of the individual dates obtained from the other 110 analyses, and in conjunction with the presence of a crack in the analysed grain, raises the possibility that the analysed site was affected by post-crystallisation loss of radiogenic Pb.

A more robust estimate of the maximum age for deposition of the host rock is derived from the 65 analyses in Group 2, which reflect a dominance of Early to Middle Permian zircon ages in the source region. The possibility that Group 2 represents a single-aged magmatic source with a weighted mean ^{204}Pb-corrected ^{238}U/^{206}Pb date of 283.1 ± 1.2 Ma (95% confidence) is precluded by the degree of scatter of the constituent analyses, which significantly exceeds that expected from the individual analytical uncertainties (MSWD = 3.4, P_{equiv} = 0.000). However, this dominant Permian 'age-peak' is not easily deconvolved into multiple age components (either visually or by mathematical means), and it is likely that the frequency maximum defined by Group 2 has geological significance, even though the constituent analyses do not conform to the Gaussian distribution assumed in the calculation of an error-weighted mean. We therefore quantify the 'central value' of the 65 ^{204}Pb-corrected ^{238}U/^{206}Pb dates in Group 2 as the median, which has a value of 282.6 +1.7/-1.3 Ma (95% confidence). This is interpreted as a robust maximum age for the youngest detrital zircon component, because in the likely event that the 65 analyses in Group 2 were derived from multiple sources with distinct ages, at least one of those sources must be younger than 282.6 +1.7/-1.3 Ma. The median date calculated for Group 2 therefore represents a conservative maximum age for deposition of the sedimentary protolith of the metasandstone.

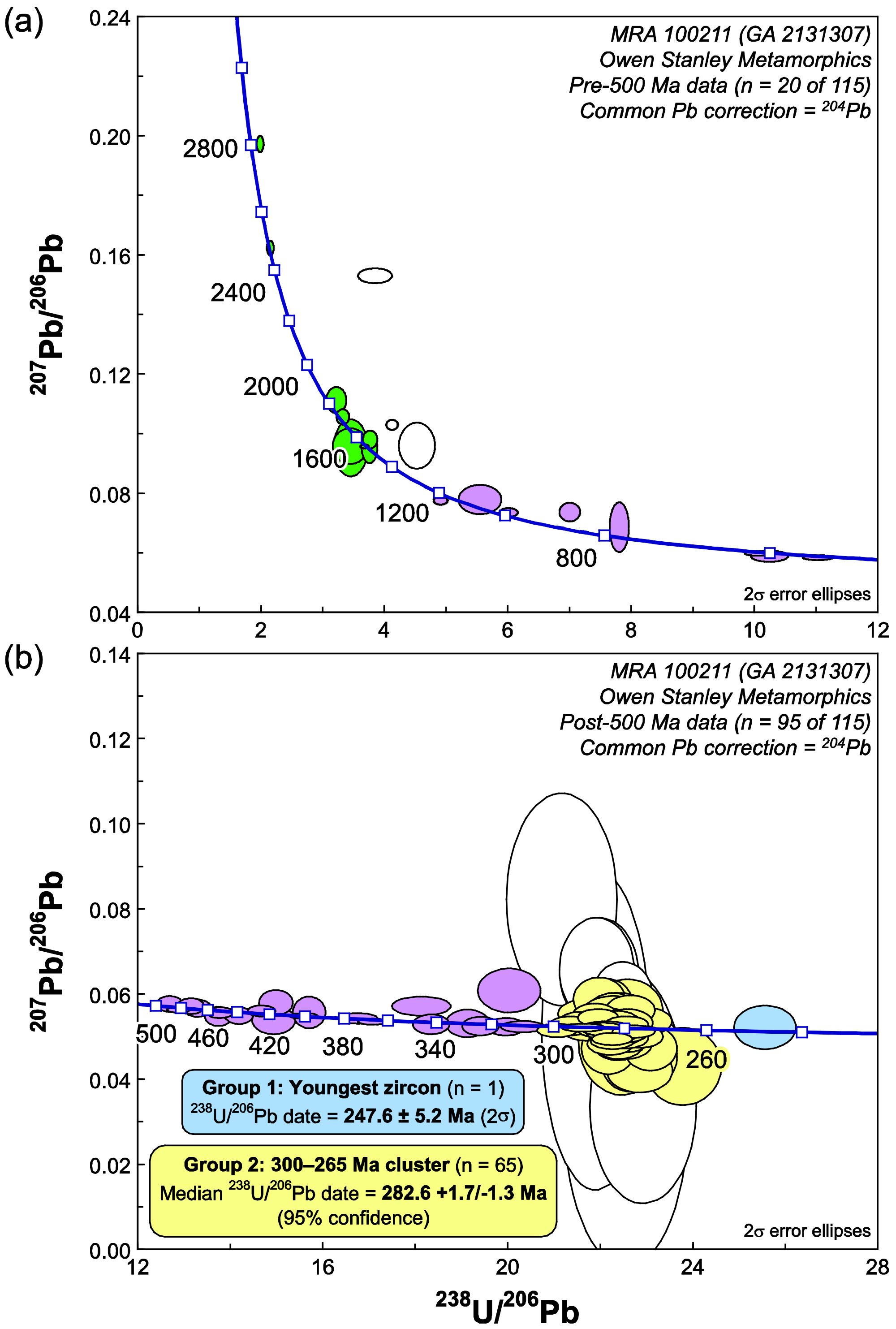

Figure 4.2 *Tera-Wasserburg concordia diagrams for SHRIMP U-Pb zircon data from the Owen Stanley Metamorphics (MRA 100211, GA 2131307). (a) Pre-500 Ma data; (b) Post-500 Ma data. Pale blue fill denotes Group 1 (youngest detrital zircon); pale yellow fill denotes Group 2 (300–265 Ma provenance cluster); pale pink fill denotes Group 3 (1200–300 Ma provenance individuals); green fill denotes Group 4 (pre-1200 Ma provenance individuals); white fill denotes analyses not considered ($^{206}Pb_c$ > 1%, $^{206}Pb_c$ < -1%, or discordance > 10% (for pre-1200 Ma data); Table 4.2).*

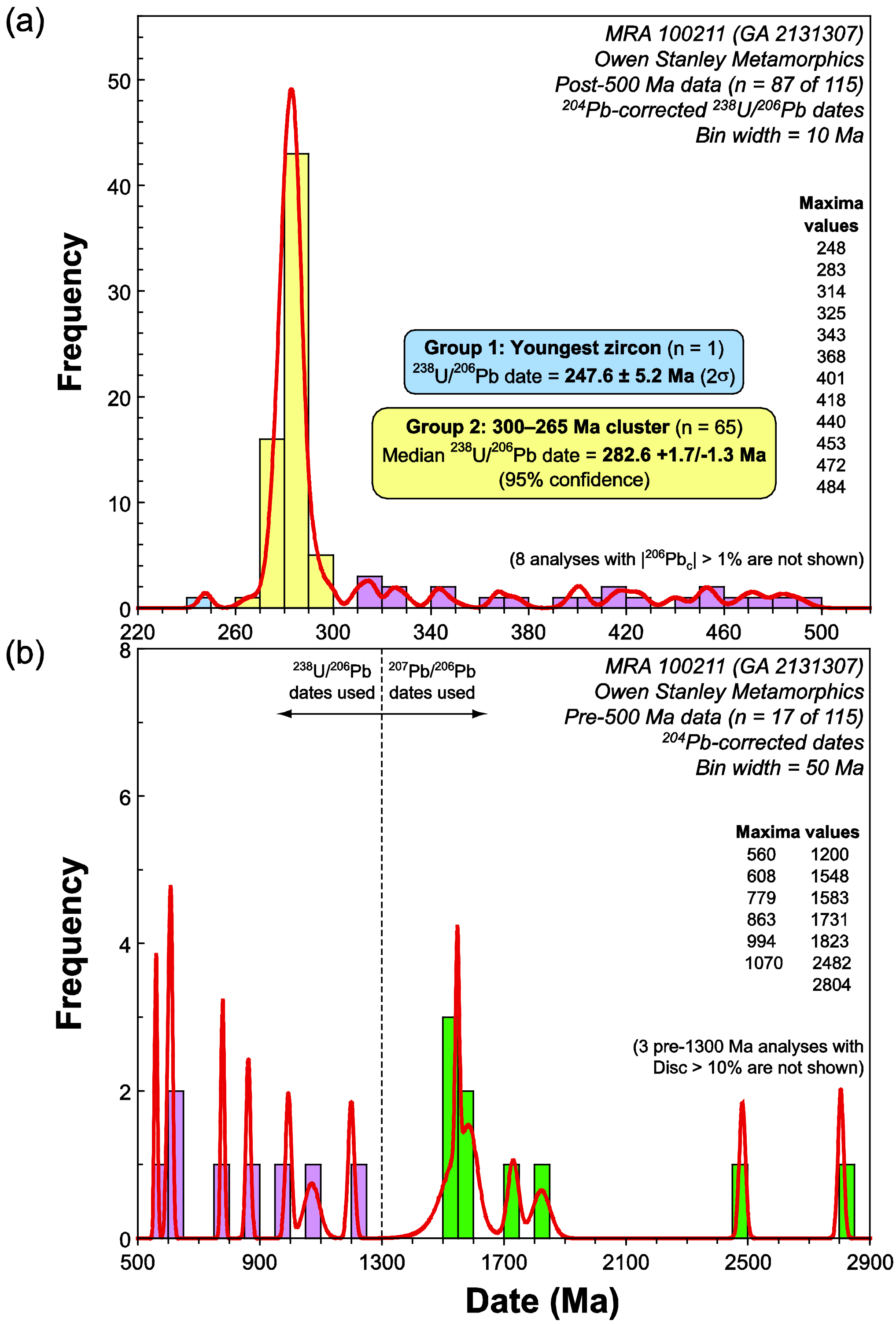

Figure 4.3 *Frequency histograms and probability density distributions for SHRIMP U-Pb zircon data from the Owen Stanley Metamorphics (MRA 100211, GA 2131307). (a) Post-500 Ma data; (b) Pre-500 Ma data. Pale blue fill denotes Group 1 (youngest detrital zircon); pale yellow fill denotes Group 2 (300–265 Ma provenance cluster); pink fill denotes Group 3 (1200–300 Ma provenance individuals); green fill denotes Group 4 (pre-1200 Ma provenance individuals). Heavy red curve: relative probability density distribution.*

The 29 analyses in Group 3 are interpreted as inherited cores and provenance individuals spanning a range of mid-Mesoproterozoic to Late Carboniferous ages, with no statistically significant clusters. Similarly, the nine analyses in Group 4 are interpreted as inherited and detrital individuals of Neoarchean to Early Mesoproterozoic age, with the youngest five analyses compatible with derivation from a single-aged source with a mean ^{204}Pb-corrected ^{207}Pb/^{206}Pb date of 1551 ± 12 Ma (95% confidence).

Table 4.2 *SHRIMP U-Pb zircon data from the Owen Stanley Metamorphics (MRA 100211, GA 2131307). Unless otherwise indicated in the Group heading, all isotopic ratios and dates are corrected for common Pb using ^{204}Pb, and all dates are ^{238}U/^{206}Pb.*

Grain.area .replicate	^{206}Pb$_c$ (%)	U (ppm)	Th (ppm)	^{232}Th /^{238}U	^{238}U /^{206}Pb	±1σ (%)	^{207}Pb /^{206}Pb	±1σ (%)	Date (Ma)	±1σ (Ma)	Disc (%)
Group 1: Youngest detrital zircon (n = 1)											
101.1.1	0.31	76	43	0.57	25.53	1.07	0.05233	3.95	247.6	2.6	18
Group 2: 300–265 Ma provenance cluster (n = 65)											
98.1.1	0.88	80	42	0.54	23.75	1.42	0.04316	8.62	265.8	3.7	—
38.1.1	0.73	99	87	0.91	23.05	1.02	0.04747	4.50	273.7	2.7	-282
41.1.1	0.90	55	47	0.88	22.97	1.19	0.04542	6.68	274.7	3.2	—
24.2.1	0.00	80	38	0.49	22.91	1.09	0.05375	2.50	275.5	2.9	24
27.1.1	0.33	230	69	0.31	22.84	0.87	0.05020	2.18	276.3	2.4	-36
36.1.1	0.82	114	77	0.70	22.83	1.27	0.04220	4.98	276.4	3.4	—
79.1.1	0.28	118	119	1.04	22.74	0.99	0.05211	2.90	277.5	2.7	4
59.1.1	0.10	514	48	0.10	22.70	0.81	0.05133	1.19	277.9	2.2	-9
108.1.1	0.28	44	36	0.84	22.67	1.23	0.04815	4.89	278.3	3.4	-164
81.1.1	0.83	79	70	0.91	22.63	1.10	0.04346	5.82	278.7	3.0	—
107.1.1	-0.34	130	81	0.64	22.63	0.95	0.05632	2.54	278.8	2.6	41
67.1.1	0.42	154	73	0.49	22.59	0.94	0.05095	2.88	279.2	2.6	-17
2.1.1	0.28	135	169	1.29	22.57	0.94	0.05021	2.92	279.4	2.6	-37
31.1.1	-0.17	110	83	0.78	22.57	0.97	0.05343	2.49	279.5	2.7	20
55.1.1	-0.41	35	41	1.20	22.56	1.38	0.05609	5.53	279.6	3.8	40
95.1.1	-0.05	303	103	0.35	22.54	0.85	0.05307	1.41	279.8	2.3	16
68.1.1	0.27	98	92	0.97	22.54	1.02	0.04876	3.31	279.8	2.8	-107
74.1.1	0.28	236	122	0.53	22.52	0.88	0.04989	2.09	280.1	2.4	-49
106.1.1	0.08	162	130	0.83	22.51	0.91	0.05124	1.96	280.2	2.5	-12
54.1.1	0.00	228	95	0.43	22.49	0.87	0.05070	1.50	280.4	2.4	-24
37.1.1	-0.26	153	103	0.69	22.48	1.22	0.05322	2.39	280.5	3.4	17
44.1.1	0.36	88	71	0.84	22.46	1.04	0.04940	3.65	280.8	2.9	-70
8.1.1	0.66	18	20	1.13	22.45	1.73	0.04907	10.45	281.0	4.8	-88
73.1.1	0.13	457	47	0.11	22.43	0.82	0.05065	2.09	281.1	2.3	-26
29.1.1	0.06	376	287	0.79	22.42	0.83	0.05148	1.20	281.3	2.3	-7

Grain.area .replicate	$^{206}Pb_c$ (%)	U (ppm)	Th (ppm)	$^{232}Th/^{238}U$	$^{238}U/^{206}Pb$	±1σ (%)	$^{207}Pb/^{206}Pb$	±1σ (%)	Date (Ma)	±1σ (Ma)	Disc (%)
9.2.1	0.16	237	29	0.13	22.41	0.87	0.05106	1.81	281.4	2.4	-16
34.1.1	-0.19	62	55	0.92	22.40	1.11	0.05600	3.24	281.6	3.1	39
25.1.1	-0.14	92	50	0.56	22.38	1.03	0.05410	2.69	281.8	2.8	25
45.1.1	0.00	180	175	1.01	22.37	0.90	0.05069	1.65	281.9	2.5	-25
33.1.1	0.38	103	65	0.65	22.37	1.00	0.04868	3.47	282.0	2.8	-116
76.1.1	0.21	101	74	0.76	22.36	1.02	0.04878	3.31	282.0	2.8	-108
94.1.1	-0.11	181	93	0.53	22.32	0.91	0.05366	1.91	282.5	2.5	21
69.1.1	0.13	346	42	0.12	22.31	0.84	0.05063	1.47	282.6	2.3	-27
65.1.1	-0.43	139	127	0.95	22.26	1.20	0.05595	2.72	283.3	3.3	38
32.1.1	-0.59	93	61	0.67	22.26	1.02	0.05570	3.50	283.3	2.8	36
23.1.1	-0.13	140	132	0.97	22.25	0.93	0.05354	3.74	283.4	2.6	20
57.1.1	0.14	571	81	0.15	22.24	0.81	0.04964	1.14	283.6	2.2	-60
100.1.1	0.14	272	185	0.70	22.23	0.86	0.04919	1.66	283.7	2.4	-82
53.1.1	0.07	255	42	0.17	22.19	0.86	0.04979	2.56	284.2	2.4	-55
17.2.1	0.22	179	35	0.20	22.19	0.91	0.04851	2.28	284.2	2.5	-132
70.1.1	0.10	195	74	0.39	22.18	0.89	0.05097	1.83	284.3	2.5	-19
60.1.1	-0.10	199	108	0.56	22.17	1.06	0.05353	1.77	284.4	3.0	19
15.1.1	0.65	81	74	0.95	22.16	1.08	0.04740	5.23	284.6	3.0	-317
7.1.1	-0.05	226	246	1.13	22.14	0.86	0.05157	1.79	284.8	2.4	-7
58.1.1	-0.05	145	133	0.94	22.14	0.94	0.05208	1.99	284.8	2.6	1
99.1.1	0.05	232	97	0.43	22.13	0.87	0.05134	1.53	284.8	2.4	-11
63.1.1	-0.06	213	202	0.98	22.13	0.88	0.05302	1.60	284.9	2.5	14
56.1.1	-0.42	139	147	1.10	22.13	1.24	0.05515	2.69	284.9	3.5	33
64.1.1	-0.08	147	52	0.37	22.12	0.93	0.05409	1.96	285.0	2.6	25
4.1.1	-0.12	160	94	0.61	22.11	0.91	0.05400	2.18	285.1	2.5	24
10.1.1	-0.68	105	59	0.58	22.11	1.01	0.05854	3.64	285.2	2.8	49
66.1.1	-0.09	454	106	0.24	22.10	1.01	0.05217	1.16	285.3	2.8	3
35.1.1	-0.31	105	59	0.58	22.05	1.00	0.05313	2.92	285.9	2.8	15
93.1.1	0.10	459	39	0.09	22.04	0.82	0.05185	1.21	286.0	2.3	-3
111.1.1	0.03	360	38	0.11	22.03	0.83	0.05192	1.21	286.2	2.3	-1
5.1.1	-0.65	153	115	0.78	22.00	1.75	0.05560	2.94	286.6	4.9	35
40.1.1	-0.74	100	66	0.68	21.96	1.04	0.05897	3.46	287.1	2.9	50
14.1.1	-0.16	388	94	0.25	21.93	0.83	0.05461	1.49	287.5	2.3	28
83.1.1	0.07	265	270	1.05	21.93	0.87	0.05198	1.54	287.5	2.4	-1
52.1.1	-0.27	191	289	1.56	21.86	0.90	0.05522	1.95	288.4	2.5	32
102.1.1	0.00	113	65	0.59	21.68	0.99	0.05182	2.06	290.7	2.8	-5
42.1.1	-0.06	837	219	0.27	21.61	0.85	0.05230	0.75	291.6	2.4	2

Grain.area .replicate	$^{206}Pb_c$ (%)	U (ppm)	Th (ppm)	$^{232}Th/^{238}U$	$^{238}U/^{206}Pb$	±1σ (%)	$^{207}Pb/^{206}Pb$	±1σ (%)	Date (Ma)	±1σ (Ma)	Disc (%)
103.1.1	-0.13	186	278	1.54	21.56	0.89	0.05364	1.71	292.2	2.5	18
1.1.1	-0.02	719	533	0.76	21.33	0.89	0.05269	1.75	295.4	2.6	6
62.1.1	0.06	361	246	0.70	21.04	0.84	0.05169	1.29	299.3	2.5	-10
Group 3: 1200–300 Ma provenance individuals (n = 29)											
30.1.1	0.09	420	141	0.35	20.29	0.95	0.05251	1.06	310.1	2.9	-1
86.1.1	0.00	33	25	0.78	20.01	1.40	0.06095	3.47	314.4	4.3	52
16.1.1	0.14	311	88	0.29	19.94	0.84	0.05249	1.63	315.5	2.6	-3
88.1.1	0.10	444	301	0.70	19.38	0.82	0.05258	1.70	324.3	2.6	-4
6.1.1	0.05	101	48	0.49	19.10	0.98	0.05327	2.48	329.0	3.1	3
22.1.1	0.29	236	84	0.37	18.31	0.87	0.05300	1.80	342.8	2.9	-4
61.1.1	-0.20	205	101	0.51	18.10	1.42	0.05732	1.63	346.7	4.8	32
9.1.1	0.02	1982	911	0.47	17.06	0.77	0.05369	0.51	367.2	2.8	-3
72.1.1	-0.02	416	269	0.67	16.74	1.01	0.05446	0.95	374.1	3.7	4
3.1.1	0.00	150	231	1.58	15.67	0.91	0.05584	2.73	398.7	3.5	11
17.1.1	0.01	1630	542	0.34	15.56	0.78	0.05504	0.45	401.6	3.0	3
92.1.1	-0.20	105	27	0.26	14.96	1.00	0.05814	2.07	417.0	4.0	23
43.1.1	0.37	111	52	0.48	14.91	1.27	0.05400	2.46	418.4	5.1	-13
82.1.1	-0.03	412	105	0.26	14.64	0.83	0.05622	0.90	425.8	3.4	8
21.1.1	0.12	210	139	0.69	14.15	0.89	0.05507	1.42	440.1	3.8	-6
85.1.1	-0.01	337	391	1.20	13.75	0.84	0.05572	0.91	452.6	3.7	-3
89.1.1	0.31	206	117	0.59	13.72	0.90	0.05493	1.70	453.5	3.9	-11
104.1.1	-0.08	366	176	0.50	13.26	0.95	0.05685	1.49	468.8	4.3	4
80.1.1	-0.14	220	172	0.81	13.12	0.88	0.05731	1.31	473.6	4.0	6
28.1.1	0.02	1268	437	0.36	12.85	0.78	0.05646	0.46	483.0	3.6	-3
91.1.1	-0.02	149	34	0.24	12.66	0.93	0.05783	1.29	490.1	4.4	7
39.1.1	0.01	704	101	0.15	11.01	0.91	0.05869	0.56	560.3	4.9	-1
90.1.1	0.02	139	260	1.93	10.23	1.20	0.05927	1.26	601.4	6.9	-4
26.1.1	0.03	771	366	0.49	10.07	0.95	0.06019	0.51	610.6	5.5	0
77.1.1	0.10	1183	271	0.24	7.79	0.79	0.06895	4.94	778.7	5.8	14
109.1.1	-0.06	141	20	0.15	6.98	0.96	0.07411	1.71	862.7	7.8	19
92.2.1	-0.01	1200	401	0.35	6.00	1.04	0.07385	0.78	994.1	9.6	4
50.1.1	-0.06	230	59	0.26	5.54	2.58	0.07817	2.54	1070.5	25.4	8
75.1.1	0.05	154	132	0.89	4.89	0.93	0.07796	0.72	1200.1	10.2	-5
Group 4: Pre-1200 Ma provenance individuals (n = 9; $^{207}Pb/^{206}Pb$ dates tabulated)											
19.1.1	0.01	198	104	0.54	3.43	3.25	0.09553	4.09	1539	77	-8
48.1.1	-0.01	537	84	0.16	3.74	1.38	0.09577	2.30	1543	43	1
47.1.1	-0.01	1137	857	0.78	3.65	0.78	0.09601	0.33	1548	6	-1

Grain.area .replicate	$^{206}Pb_c$ (%)	U (ppm)	Th (ppm)	^{232}Th /^{238}U	^{238}U /^{206}Pb	±1σ (%)	^{207}Pb /^{206}Pb	±1σ (%)	Date (Ma)	±1σ (Ma)	Disc (%)
20.1.1	-0.02	644	51	0.08	3.43	3.38	0.09617	2.54	1551	48	-7
11.1.1	-0.01	353	97	0.29	3.74	1.26	0.09833	1.27	1593	24	5
13.1.1	0.01	285	173	0.63	3.30	1.23	0.10595	0.98	1731	18	2
96.1.1	0.11	197	94	0.49	3.19	2.09	0.11145	1.60	1823	29	4
87.1.1	0.03	114	56	0.51	2.13	0.98	0.16250	0.61	2482	10	0
97.1.1	-0.01	358	191	0.55	1.96	1.03	0.19736	0.57	2804	9	6
Not considered: Pre-1200 Ma analyses with discordance > 10% (n = 3; $^{207}Pb/^{206}Pb$ dates tabulated)											
24.1.1	0.02	500	45	0.09	4.50	2.66	0.09623	3.24	1552	61	18
78.1.1	0.02	546	226	0.43	4.11	0.96	0.10315	0.67	1682	12	18
51.1.1	0.00	786	278	0.37	3.83	2.94	0.15315	0.67	2381	11	42
Not considered: $^{206}Pb_c$ > 1% (n = 4)											
49.1.1	2.76	17	14	0.81	22.89	2.06	0.03384	27.62	275.6	5.6	—
12.1.1	3.87	13	9	0.68	22.54	2.41	0.03096	45.85	279.8	6.6	—
110.1.1	1.44	147	118	0.83	22.34	0.97	0.05300	5.56	282.3	2.7	14
105.1.1	3.68	207	179	0.89	21.87	2.18	0.05182	29.68	288.2	6.2	-4
Not considered: $^{206}Pb_c$ < -1% (n = 4)											
18.1.1	-1.34	62	61	1.02	22.46	1.18	0.05977	5.42	280.8	3.2	54
46.1.1	-1.75	27	31	1.18	21.95	1.57	0.06508	8.09	287.2	4.4	64
84.1.1	-1.65	34	25	0.78	21.90	1.51	0.06589	7.57	287.8	4.2	66
71.1.1	-3.40	14	8	0.62	21.14	2.31	0.08230	12.39	297.9	6.7	78

5. Discussion

This brief Discussion is aimed at evaluating the new SHRIMP U-Pb zircon results with respect to each other, and in the context of previous U-Pb, K-Ar and Rb-Sr isotopic studies. The regional geological implications of the results will be discussed elsewhere.

5.1. Bulolo Volcanics

The two samples from the Bulolo Volcanics establish maximum and minimum ages on the eruptive event. The magmatic crystallisation age of 3.46 ± 0.06 Ma (95% confidence) derived from the 'bomb' of porphyritic andesite hosted by a volcanic breccia (MRA 100214, GA 2131308) defines a maximum age for deposition of the host breccia, although widespread evidence for high-temperature emplacement of other breccia-hosted bombs (such as chilled and crenulate margins, sac shapes, and bombs flattened against each other) within the same exposure indicates that the host breccia was probably deposited at about the same time as the 'bomb' crystallised (Saroa et al., 2012). Similarly, the magmatic crystallisation age of 3.22 ± 0.06 Ma (95% confidence) obtained from the subvolcanic diorite (MRA 100338, GA 2131310) defines a minimum age for deposition of the volcanic breccia it intrudes. The two dates are distinguishably different at the 95% confidence level (MSWD = 32, P_{equiv} = 0.000), and occur in the correct order with respect to the relative event framework, so accumulation of the Bulolo Volcanics occurred between 3.46 ± 0.06 Ma and 3.22 ± 0.06 Ma, corresponding to an interval of 0.24 ± 0.08 million years duration.

These results are in excellent agreement with a multi-sample plagioclase K-Ar isochron age of 3.39 ± 0.22 Ma determined by Page and McDougall (1972). Many of the sample-specific plagioclase and biotite K-Ar determinations yielded apparent ages older than 3.5 Ma (and older than 6 Ma in some cases), so the new U-Pb zircon data corroborate the suggestion by Page and McDougall (1972) that most of the analysed plagioclases and biotites incorporated extraneous (inherited) argon into their lattices at the time of crystallisation.

5.2. Morobe Granodiorite

The new magmatic crystallisation age of 13.62 ± 0.13 Ma obtained from the Morobe Granodiorite in the western Kuper Range (MRA 100417, GA 2131311) is slightly older than the existing K-Ar determinations available from a single sample in each of the main masses of the Morobe pluton: 12.6 ± 0.3 Ma (hornblende) from nearby in the western Kuper Range, and 12.3 ± 0.3 Ma (hornblende) and 11.0 ± 0.2 Ma (biotite) in the eastern Ekuti Range, south of Wau (Dow et al., 1974; Page, 1976). However, the new zircon age is consistent with a larger body of K-Ar and Rb-Sr data from the smaller Watut, Sunshine and Gurukar masses (exposed to the north and west of the Ekuti and Kuper ranges), which yielded multi-sample K-Ar isochrons of 14.8 ± 1.3 Ma (hornblende) and 13.2 ± 0.7 Ma (biotite), as well as three sample-specific biotite Rb-Sr determinations spanning the range 14.5–12.7 Ma (Page, 1976). The agreement of these U-Pb, K-Ar and Rb-Sr results suggests that the Ekuti and Kuper plutons are the same age as the Watut, Sunshine and Gurukar plutons, with the apparent disparity in K-Ar hornblende ages being an artefact of lower data density in the Ekuti and Kuper masses.

The SHRIMP U-Pb analyses also revealed the existence of inherited zircon (as cores with Miocene magmatic overgrowths, and as discrete xenocrysts), with six analyses comprising (i) a cluster of three with an age of 233.9 ± 4.0 Ma, (ii) two analyses within error of each other at 186.7 ± 4.1 Ma, and (iii) a single analysis at c. 397 Ma. This cluster of U-Pb zircon ages at c. 234 Ma is similar to SHRIMP U-Pb zircon ages of 244.8 ± 4.9 Ma and 239.1 ± 4.2 Ma constraining magmatic crystallisation of the Kubor Granodiorite of western Papua New Guinea, some 300–500 km west-northwest of the Morobe Granodiorite (Van Wyck and Williams, 2002). The Kubor Granodiorite has also yielded six single-sample muscovite and biotite Rb-Sr dates spanning the range 244–225 Ma, as well as multi-sample K-Ar isochron ages of 226 ± 4 Ma from hornblende, 222 ± 10 Ma from biotite, and 219 ± 7 Ma from muscovite (Page, 1976). Similarly, the pair of U-Pb zircon analyses at c. 187 Ma resembles three multi-sample whole-rock Rb-Sr isochrons determined by Page (1976): 177 ± 27 Ma from aplites intruding the Kubor Granodiorite, 172 ± 27 Ma from deformed granites intruding the Bena Bena Formation east of Goroka, and 190 ± 3 Ma from the Urabagga granodiorites and diorites west of Goroka. The latter two units are located some 200–250 km northwest of the Morobe Granodiorite.

These results and comparisons suggest that Triassic and Jurassic felsic igneous rocks analogous to those exposed in western Papua New Guinea (or siliciclastic sedimentary rocks derived via erosion of those Mesozoic plutons) were present in the Miocene source region of the Morobe Granodiorite.

5.3. Owen Stanley Metamorphics

A total of 115 SHRIMP U-Pb analyses were obtained from the zircon-bearing metasandstone of the Owen Stanley Metamorphics (MRA 100211, GA 2131307). A solitary analysis yielded an earliest Triassic age (247.6 ± 5.2 Ma; 2σ), and may represent a maximum age for deposition of the precursor sandstone, as this date does not violate any independent geological constraint on the age(s) of the protoliths of the Owen Stanley Metamorphics. However, in the absence of statistical support from the rest of the dataset, the analysed zircon may have been affected (in isolation) by post-crystallisation loss of radiogenic Pb, and therefore does not define a robust maximum age for precursor sandstone deposition. The remainder of the provenance spectrum is dominated by Permian detritus, with 65 analyses yielding ages between c. 300 Ma and c. 265 Ma, and we prefer the median age of this large cluster (282.6 +1.7/-1.3 Ma; 95% confidence) as a conservative estimate of the maximum age of deposition. A further 38 analyses yielded a diverse range of Late Carboniferous (c. 310 Ma) to Neoarchean (c. 2804 Ma) ages, with only one statistically significant cluster of five analyses at 1551 ± 12 Ma.

This detrital zircon age spectrum bears a strong resemblance to that obtained via SHRIMP U-Pb analysis of zircons from a metagreywacke within the Omung Metamorphics some 220 km to the northwest (Van Wyck and Williams, 2002; their sample 625). Both provenance spectra display:

- a dominant Permian component (35–60% of all analyses) supplemented by a minor Early Triassic contribution
- no reliable ages younger than c. 230 Ma
- frequent but dispersed zircons of Early Ordovician to Late Carboniferous age (20–35% of all analyses)
- very few analyses yielding dates in the range 1500–500 Ma (2–8% of all analyses)
- a statistically significant cluster with a mean date of c. 1550 Ma (5–11% of all analyses)
- minor Neoarchean to Paleoproterozoic components (4–16% of all analyses)

Zircon-bearing magmatic rocks with ages comparable to most of the peaks in the detrital zircon age spectrum from the Owen Stanley Metamorphics (and Omung Metamorphics) are known from northeastern Australia. Permian and Late Carboniferous felsic rocks are significant components of the northern New England Orogen and the Drummond Basin in eastern Queensland (e.g. Carson et al., 2006; Cross et al., 2009, 2012, and references therein), and magmatic rocks of Neoproterozoic to Devonian age have been dated in the predominantly subsurface Thomson Orogen (e.g. Glen et al., 2010; Carson et al., 2011; Neumann and Kositcin, 2011), which flanks the New England Orogen on its western side, and defines the eastern margin of the Proterozoic Mount Isa Inlier in northwestern Queensland. Felsic rocks of Early Mesoproterozoic age (c. 1550 Ma) are known in the Mount Isa Inlier, but are more widespread in the Georgetown and Coen inliers of northeastern Queensland (e.g. Van Wyck and Williams, 2002; Neumann and Fraser, 2007, and references therein). All of these Proterozoic provinces represent potential sources for the pre-1500 Ma zircon detritus in the Owen Stanley Metamorphics.

The strong similarity between the age spectra analysed from the Owen Stanley and Omung Metamorphics raises the possibility that protoliths of the Omung Metamorphics form part of the Owen Stanley Metamorphics. If this correlation is valid, then the minimum age for protolith deposition of the Omung Metamorphics (provided by the cross-cutting c. 240 Ma Kubor Granodiorite: Page, 1976; Van Wyck and Williams, 2002) might also apply to the analysed metasandstone from the Owen Stanley Metamorphics. This would explain the absence of mid-Triassic and younger zircons from its provenance spectrum, despite post-230 Ma felsic magmatic rocks being widespread in the proposed source region (e.g. Carson et al., 2006; Cross et al., 2009, 2012).

Acknowledgements

Geological mapping and sampling by MRA in the Wau-Bulolo area in September 2011 was carried out with the permission of local government authorities, tenement holders, and landowners, and with the assistance of numerous villagers and local guides. Ricky Yatapsa's local knowledge and driving skills were invaluable during the field work.

The SHRIMP zircon U-Pb analytical program was conducted using high quality zircon separates, mounts, photographs and cathodoluminescence images professionally and skilfully prepared by David DiBugnara, Benjamin Linehan, and Rick Long of GA's Mineral Separation Laboratory. Patrick Burke provided valuable technical support and assistance in optimising analytical conditions on the GA SHRIMP IIe during data acquisition. Formal reviews of this report by Andrew Cross and Natalie Kositcin (GA) resulted in important improvements.

References

Bodorkos, S., Beyer, E.E., Edgoose, C.J., Whelan, J.A., Webb, G., Vandenberg, L.C. and Hallett, L., 2013. *Summary of results. Joint NTGS-GA geochronology project: Central and East Arunta regions, January 2008–June 2011.* Northern Territory Geological Survey Record 2013-003.

Bodorkos, S., Blevin, P.L., Simpson, C.J., Gilmore, P.J., Glen, R.A., Greenfield, J.E., Hegarty, R. and Quinn, C.D., in press. *New SHRIMP U-Pb zircon ages from the Lachlan, Thomson and Delamerian orogens, New South Wales, July 2009–June 2010.* Geoscience Australia Record–Geological Survey of New South Wales Report.

Carson, C.J., Hollis, J.A., Glass, L.M., Close, D.F., Whelan, J.A. and Wygralak, A., 2010. *Summary of results. Joint NTGS-GA geochronology project: Arunta, Pine Creek regions July 2007–July 2009.* Northern Territory Geological Survey Record 2010-004.

Carson, C.J., Hutton, L.J., Withnall, I.W., Perkins, W.G., Donchak, P.J.T., Parsons, A., Blake, P.R., Sweet, I.P., Neumann, N.L. and Lambeck, A., 2011. *Joint GSQ–GA geochronology project, Mount Isa region, 2009–2010.* Queensland Geological Record 2011/03.

Carson, C.J., von Gnielinski, F.E. and Bultitude, R.J., 2006. *Results of the joint GSQ–GA geochronology project, New England Orogen: Rosedale, Mount Perry and Gladstone 1:100 000 sheet areas, March 2006–December 2006.* Queensland Geological Record 2006/01.

Carswell, J.T., 1990. Wau gold deposits. *In* Hughes, F.E., editor, *Geology of the Mineral Deposits of Australia and Papua New Guinea.* Australasian Institute of Mining and Metallurgy Monograph Series 14, pp. 1763–1767.

Claoué-Long, J.C., Compston, W., Roberts, J. and Fanning, C.M., 1995. Two Carboniferous ages: a comparison of SHRIMP zircon dating with conventional zircon ages and $^{40}Ar/^{39}Ar$ analysis. *In* Berggren, W.A., Kent, D.V., Aubry, M.-P. and Hardenbol, J., editors, *Geochronology, Time Scales and Global Stratigraphic Correlation.* SEPM Special Publication 54, pp. 3–21. Society for Sedimentary Geology, Tulsa, Oklahoma, USA.

Compston, W., Williams, I.S. and Meyer, C., 1984. U-Pb geochronology of zircons from lunar breccia 73217 using a sensitive high-mass resolution ion microprobe. *Journal of Geophysical Research* 89 (Supplement), B525–B534.

Cross, A.J., Purdy, D.J. and Bultitude, R.J., 2012. *Summary of results — joint GSQ–GA geochronology project: Monto and Maryborough 1:250 000 sheet areas.* Queensland Geological Record 2012/02.

Cross, A.J., Purdy, D.J., Bultitude, R.J., Dhnaram, C.R. and von Gnielinski, F.E., 2009. *Joint GSQ–GA NGA geochronology project: New England Orogen and Drummond Basin.* Queensland Geological Record 2009/03.

Cussen, M.J., Wangu, A., McCulla, M.S. and Tau Loi, D., 1986. *Geology and mineralisation of the Wau area, Papua New Guinea.* Geological Survey of Papua New Guinea Report 86/16.

Dow, D.B., Smit, J.A.J. and Page, R.W., 1974. *Wau, Papua New Guinea 1:250 000 Geological Series (SB55-14) Explanatory Notes.* Bureau of Mineral Resources, Canberra.

Fisher, N.H., 1944. Outline of the geology of the Morobe goldfield. *Proceedings of the Royal Society of Queensland* 55, 51–58.

Glen, R.A., Saeed, A., Hegarty, R., Percival, I.G., Bodorkos, S. and Griffin, W.L., 2010. *Preliminary zircon data and tectonic framework for the Thomson Orogen, northwestern NSW.* Geological Survey of New South Wales Report GS2010/0379.

Hoaglin, D.C., Mosteller, F. and Tukey, J.W., 1983. *Understanding Robust and Exploratory Data Analysis.* John Wiley and Sons, New York, pp. 345–349.

Jaffey, A.H., Flynn, K.F., Glendenin, L.E., Bentley, W.C. and Essling, A.M., 1971. Precision measurement of half-lives and specific activities of ^{235}U and ^{238}U. *Physical Review C* 4, 1889–1906.

Ludwig, K.R., 2009. *SQUID 2 Rev. 2.50: A User's Manual.* Berkeley Geochronology Center Special Publication 5.

Ludwig, K.R., 2003. *User's Manual for Isoplot 3.6* (April 2008 revision). Berkeley Geochronology Center Special Publication 4.

Mackay, N.J., 1955. *Geological report on a reconnaissance of the Markham and Upper Ramu drainage systems, New Guinea.* Bureau of Mineral Resources, Geology and Geophysics Record 1955/25.

Nasdala, L., Hofmeister, W., Norberg, N., Mattinson, J.M., Corfu, F., Dörr, W., Kamo, S.L., Kennedy, A.K., Kronz, A., Reiners, P.W., Frei, D., Kosler, J., Wan, Y., Götze, J., Häger, T., Kröner, A. and Valley, J.W., 2008. Zircon M257 – a homogeneous natural reference material for the ion microprobe U–Pb analysis of zircon. *Geostandards and Geoanalytical Research* 32, 247–265.

Nelson, D.R., 1997. *Compilation of SHRIMP U-Pb zircon geochronology data, 1996.* Geological Survey of Western Australia Record 1997/2.

Neumann, N.L. and Fraser, G.L., 2007. *Geochronological synthesis and time-space plots for Proterozoic Australia.* Geoscience Australia Record 2007/06.

Neumann, N.L. and Kositcin, N., 2011. *New SHRIMP U-Pb zircon ages from north Queensland, 2007–2010.* Geoscience Australia Record 2011/38.

Page, R.W., 1976. *Geochronology of igneous and metamorphic rocks in the New Guinea Highlands.* Bureau of Mineral Resources Bulletin 162.

Page, R.W. and McDougall, I., 1972. Ages of mineralization of gold and porphyry copper deposits in the New Guinea Highlands. *Economic Geology* 67, 1034–1048.

Pieters, P.E., 1978. *Port Moresby–Kalo–Aroa, Papua New Guinea 1:250 000 Geological Series Explanatory Notes.* Bureau of Mineral Resources, Geology and Geophysics, Canberra.

Pigram, C.J. and Davies, H.L., 1987. Terranes and accretion history of the New Guinea orogen. *BMR Journal of Australian Geology & Geophysics* 10, 193–211.

Plane, M.D., 1967. *Stratigraphy and vertebrate fauna of the Otibanda Formation, New Guinea.* Bureau of Mineral Resources Bulletin 86.

Rock, N.M.S., Webb, J.A., McNaughton, N.J. and Bell, G.D., 1987. Nonparametric estimation of averages and error for small data-sets in isotope geoscience: a proposal. *Chemical Geology* 66, 163–177.

Rogerson, R. and Francis, G., 1983. Owen Stanley Metamorphic Complex type of initial prograde metamorphism. *Science in New Guinea* 10, 60–64.

Saroa, D., Tsiperau, C.U., Abiari, I., Bokuik, A.L., Kuman, N., Lahan, M.M., Poke, B., Tevlone, A.P. and Sheppard, S., 2012. *A preliminary re-examination of the geology of the Wau–Bulolo area*. Mineral Resources Authority, Papua New Guinea Technical Note TN 2012/03.

Sillitoe, R.H., Baker, E.M. and Brooks, W.A., 1984. Gold deposits and hydrothermal eruption breccia associated with a maar volcano at Wau, Papua New Guinea. *Economic Geology* 79, 638–655.

Sircombe, K.N., Cassidy, K.F., Champion, D.C. and Tripp, G., 2007. *Compilation of SHRIMP U-Pb geochronological data: Yilgarn Craton, Western Australia, 2004–2006.* Geoscience Australia Record 2007/01.

Stacey, J.S. and Kramers, J.D., 1975. Approximation of terrestrial lead isotope evolution using a two-stage model. *Earth and Planetary Science Letters* 26, 207–221.

Steiger, R.H. and Jäger, E., 1977. Subcommission on geochronology: convention on the use of decay constants in geo- and cosmochronology. *Earth and Planetary Science Letters* 36, 359–362.

Stern, R.A. and Amelin, Y., 2003. Assessment of errors in SIMS zircon U–Pb geochronology using a natural zircon standard and NIST SRM 610 glass. *Chemical Geology* 197, 111–142.

Stern, R.A., Bodorkos, S., Kamo, S.L., Hickman, A.H. and Corfu, F., 2009. Measurement of SIMS instrumental mass fractionation of Pb isotopes during zircon dating. *Geostandards and Geoanalytical Research* 33, 145–168.

Van Wyck, N. and Williams, I.S., 2002. Age and provenance of basement metasediments from the Kubor and Bena Bena Blocks, central Highlands, Papua New Guinea: constraints on the tectonic evolution of the northern Australian cratonic margin. *Australian Journal of Earth Sciences* 49, 565–577.

Williams, I.S., 1998. U-Th-Pb geochronology by ion microprobe. *In* McKibben, M.A., Shanks III, W.C. and Ridley, W.I., editors, *Applications of Microanalytical Techniques to Understanding Mineralizing Processes.* Reviews in Economic Geology 7, 1–35. Society of Economic Geologists, Littleton, Colorado, USA.

Williams, I.S., Buick, I.S. and Cartwright, I., 1996. An extended episode of early Mesoproterozoic metamorphic fluid flow in the Reynolds Range, central Australia. *Journal of Metamorphic Geology* 14, 29–47.

Williamson, A. and Hancock, G. (editors), 2005. *The Geology and Mineral Potential of Papua New Guinea.* Papua New Guinea Department of Mining.

Worthing, M.A., 1988. Petrology and tectonic setting of blueschist facies metabasites from the Emo Metamorphics of Papua New Guinea. *Australian Journal of Earth Sciences* 35, 159–168.

Appendix A. SHRIMP Data Acquisition, Reduction and Presentation

A.1. Analytical Procedures

All isotopic analyses reported in this report were undertaken using the SHRIMP IIe at GA, in Canberra. A summary of key parameters from individual analytical sessions are shown in Appendix Table A.1. The analytical procedures adopted (and outlined below) for zircon follow those published by Compston et al. (1984), Claoué-Long et al. (1995), Nelson (1997), and Williams (1998).

A.1.1. Sample Acquisition and Crushing

The locations of field sites were determined using hand-held GPS units with accuracies of about 100 metres, and are referred to the World Geodetic System 1984 (WGS84). Co-ordinates are reported as decimal latitude and longitude, and as Universal Transverse Mercator (UTM) eastings and northings (UTM Zone 55). Sites and samples are labelled using the relevant identifiers in each of the corporate systems: MRA SiteID and SampleNo, and GA SampleNo.

All samples were obtained from outcrop, with slabs and boulders split via sledgehammer to access the freshest available rock. Samples were submitted to the Mineral Separation Laboratory at GA, where residual weathered rock was removed from each sample, yielding a mass of fresh rock in the range 1–3 kg. Each fresh sample was pulverised (to 2–5 cm pieces) using a pre-cleaned hydraulic splitter, ultrasonically washed in water, and dried under heat lamps. Samples were then crushed using a Rocklabs Boyd crusher, and milled using a Rocklabs continuous ring mill.

A.1.2. Mineral Separation

Mineral-density separation was undertaken using a Wilfley table, with multiple iterations employed in order to successively deslime the rock flours and decant bulk low-density minerals such as quartz and feldspar, thereby reducing the sample to about 5% of its post-milling weight. Strongly paramagnetic grains were successively removed from this heavy fraction using a ferrous magnet and a rare-earth element magnet, before the remainder underwent a series of magnetic separations using a Frantz barrier separator. This typically involved 6–8 separations in total, with adjustments (firstly to the magnet current, and secondly to the horizontal tilt of the ramp) aimed at the sequential removal of minerals with progressively weaker paramagnetism.

In cases where the initial Frantz separation (aimed at removing the most strongly paramagnetic material) demonstrated that the bulk of the heavy fraction was only weakly paramagnetic, the heavy fraction was immersed in liquid diiodomethane (specific gravity 3.3), in order to further reduce the low-density mineral content before the remaining Frantz separations were carried out. Where available, 300–400 zircons were hand-picked for each sample, commencing with grains in the least magnetic fraction, and progressing to successively more magnetic fractions in samples with low yield, without any discrimination based on the external morphologies of the grains.

Appendix Table A.1 *Summary of session-specific metadata, parameters obtained from $^{238}U/^{206}Pb$ and $^{207}Pb/^{206}Pb$ reference zircons, and samples analysed.*

	Session 120071	Session 120088
MountID	GA6211	GA6211
Session dates	27 Sep–1 Oct 2012	1–5 Nov 2012
$^{238}U/^{206}Pb$ reference zircon	AusZ2 (38.86 Ma)	TEMORA2 (416.8 Ma)
Analyses used	50 of 50	38 of 38
Slope of robust regression (95% confidence): spot age (Ma) / session duration (hours)	-0.011 +0.005/-0.006 (drift correction applied)	-0.022 +0.043/-0.040 (no correction)
$^{238}U/^{206}Pb$ session-to-session error (2σ)	0.55%	0.22%
$^{238}U/^{206}Pb$ spot-to-spot error (2σ)	2.48%	1.50% [from 0.81%]
Index isotope for common Pb correction	^{207}Pb	^{204}Pb
Mean $^{207}Pb/^{206}Pb$ date (Ma, 95% confidence)	—	415 ± 29
Mean ^{204}Pb overcounts/second from ^{207}Pb (95% confidence)	—	+0.002 ± 0.024 (no correction)
$^{207}Pb/^{206}Pb$ reference zircon	OG1 (3465.4 Ma)	OG1 (3465.4 Ma)
Analyses used	20 of 20	20 of 20
Mean $^{207}Pb/^{206}Pb$ date (Ma, 95% confidence)	3465.4 ± 1.8 (no correction)	3467.4 ± 1.4 (no correction)
Number of samples co-analysed	3	1
MRA SampleNo (GA SampleNo)	100214 (2131308)	100211 (2131307)
MRA SampleNo (GA SampleNo)	100338 (2131310)	—
MRA SampleNo (GA SampleNo)	100417 (2131311)	—

A.1.3. Mount Preparation

Hand-picked zircon separates were placed in sample-specific rows on a single strip of adhesive tape, along with two rows of the Devonian $^{238}U/^{206}Pb$ reference zircon TEMORA2 (Black et al., 2004), one row of the Eocene $^{238}U/^{206}Pb$ reference zircon AusZ2 from the Glen Innes region of New South Wales, Australia (A.K. Kennedy, written communication 2012), one row of the Archean $^{207}Pb/^{206}Pb$ reference zircon OG1 (Stern et al., 2009), and one fragment of the Neoproterozoic gem zircon M257 from Sri Lanka (Nasdala et al., 2008) as a uranium concentration reference material. The grains were then mounted in a 25 mm-diameter epoxy disc (Geoscience Australia mount GA6211), and once cured, the mount surface was polished using a series of successively finer diamond suspensions, in order to expose longitudinal sections of the crystals. The grain-rows were photographed in transmitted light, and in reflected light with differential interference contrast (DIC), using a Leica DFC310FX camera attached to a Leica DM6000M polarising microscope with automated stage. The polished surface was coated with a 20 Å thickness of high-purity (99.999%) gold, and cathodoluminescence (CL) images were acquired with GA's JEOL JSM-6490LV scanning electron microscope (SEM), using an accelerating voltage of 15 keV and a Robinson CL detector.

The gold coat was removed using a Bemcot cotton wipe saturated with ethanol, and the mount surface was ultrasonically cleaned using ethanol, propanol, petroleum spirit, and a detergent solution (comprising 10% RBS35 in deionised water), prior to quadruple-rinsing in Milli-Q water (Type 1 lab purity), in order to minimise the amount of non-radiogenic Pb contamination on the polished surface prior to analysis. The mount was dried overnight in an oven at 30°C, then recoated with a 150 Å thickness of high-purity (99.999%) gold, to facilitate the establishment of a homogeneous electric potential across the surface during analysis, thereby avoiding charge buildup. Finally, the mount was loaded into the high-vacuum sample lock of the SHRIMP 24 hours prior to commencement of the analytical session, to facilitate degassing of any remaining volatile species, and to minimise the potential for hydride residues on the mount surface.

A.1.4. Instrument Setup and Data Acquisition

A 30–40 µm-diameter primary beam of O_2^- ions at 10 keV, purified by means of a Wien filter to minimise the presence of OH^- species, was employed to sputter secondary ions from the surface of the zircons. Before each analysis, the surface of the analysis site was pre-cleaned by rastering of the primary beam for 2–3 minutes, in order to reduce the amount of common Pb on the mount surface. The total ion current measured at the mount surface was typically between 3.0 nA (session 120071) and 3.3 nA (session 120088), and uniform ion flux across each spot area was achieved by Kohler focusing of the primary beam, which resulted in even, flat-bottomed pits about 1–2 µm deep. Secondary ions were extracted through a low gradient electrostatic field (~4 keV/cm), accelerated to 10 keV, and steered firstly through a double-focusing cylindrical 85° electrostatic analyser with a turning radius of 1.27 m, and secondly through a 72.5° magnet sector with a turning radius of 1 m. Ion currents of the relevant secondary species were then determined by switching the magnetic field to direct the secondary ion beam into a single electron multiplier with a deadtime of 25 ns. Mass resolution (M/ΔM at 1% peak height, as measured on ^{208}Pb on Pb-rich feldspar from Broken Hill) exceeded 5000, and $^{206}Pb^+$-ion sensitivity (as measured on M257, which contains about 66 ppm ^{206}Pb) was approximately 25 cps/ppm/nA in session 120071 and 27 cps/ppm/nA in session 120088, assuming that the incident primary beam is usually responsible for about 70% of the total ion current measured at the mount surface during zircon analysis.

Data acquisition involved cycling the magnetic field through a run-table comprising the following ten nominal mass-stations and counting times: $^{196}Zr_2O$ (2 s), ^{204}Pb (20 s), background 204.1 (20 s), ^{206}Pb (50/60 s), ^{207}Pb (20/30 s), ^{208}Pb (5 s), ^{238}U (5 s), ^{248}ThO (2 s), ^{254}UO (2 s), and $^{270}UO_2$ (2 s). Measurement positions for the five mass-stations expected to have low count rates (^{204}Pb, background 204.1, ^{206}Pb, ^{207}Pb and ^{208}Pb) were fixed relative to the position of $^{196}Zr_2O$. A full cycle through the mass-stations is termed a scan, and the five mass-peaks expected to have high count rates ($^{196}Zr_2O$, ^{238}U, ^{248}ThO, ^{254}UO and $^{270}UO_2$) were each re-centred once per scan. Each analysis comprised six sequential scans, and typically took about 25 minutes to complete (including pre-cleaning and beam-tuning prior to the first scan).

Analyses of the three igneous samples in session 120071 were collected in 'round-robin' fashion, with the analytical sequence comprising one measurement from each sample in turn, followed by one measurement of each of the $^{238}U/^{206}Pb$ reference zircons (AusZ2 and TEMORA2) and, on every second iteration of the loop, one measurement of the $^{207}Pb/^{206}Pb$ reference zircon OG1. Analysis of the single metasedimentary sample in session 120088 did not utilise AusZ2; instead, one analysis of TEMORA2 was made after every third unknown analysis, and one analysis of OG1 was made after every second TEMORA2 analysis.

In this report, labels for individual zircon analyses (as shown in the analytical data-tables) take the form X.Y.Z, where X is the 'grain number' (usually assigned sequentially within a sample, at the time of analysis), Y is the 'area number' within grain X (used to distinguish between spots at different locations within the same grain), and Z is the 'replicate number' within area Y (used to distinguish between multiple analyses at the same location in the same grain). Nowhere in this report have multiple analyses been made at the same location in the same grain, so Z is 1 for all analyses.

A.2. Data Reduction and Presentation

Data from the SHRIMP were reduced, calculated and portrayed using Microsoft Excel® 2003, and the add-ins SQUID 2.50.11.02.03 (February 2011 revision of Ludwig, 2009) and Isoplot 3.71.09.05.23 (May 2009 revision of Ludwig, 2003). The decay constants used are those of Jaffey et al. (1971), together with present-day ^{238}U/^{235}U = 137.88, following Steiger and Jäger (1977).

All unknown analyses were corrected for common Pb, with the method employed dictated by the ages of the individual targets. Zircons of Cenozoic age are characterised by essentially uniform radiogenic ^{207}Pb/^{206}Pb, so the fraction of common ^{206}Pb as a percentage of total measured ^{206}Pb (denoted $^{206}Pb_c$ in the analytical data-tables) was estimated using the '^{207}Pb-correction', best documented by Williams (1998). This assumes that the analysed U-Pb system is concordant, and in this study, we assume that the composition of any non-radiogenic ^{207}Pb/^{206}Pb is well approximated by the model bulk-Earth value of equivalent age, as calculated using the single-stage Pb isotopic evolution model of Stacey and Kramers (1975). In contrast, $^{206}Pb_c$ values for zircons of Mesozoic and older age were estimated using the '^{204}Pb-correction', which utilises the measured ^{204}Pb/^{206}Pb and makes no assumption regarding U-Pb concordance, assuming that the ^{204}Pb/^{206}Pb value of the non-radiogenic Pb is well approximated by the model bulk-Earth value of equivalent age, following Stacey and Kramers (1975).

It is important to note that the content of the analytical data-tables is directly related to the common Pb correction employed. For analyses yielding Cenozoic dates, the tabulated isotopic ratios (^{238}U/^{206}Pb and ^{207}Pb/^{206}Pb) are *not* corrected for common Pb, although the tabulated dates (and the mean and median dates derived from them) *are* corrected for common Pb, using the ^{207}Pb-correction method. No discordance values are specified as no radiogenic ^{207}Pb/^{206}Pb value can be calculated when the ^{207}Pb-correction method has been employed. In contrast, for analyses yielding Mesozoic and older dates, the tabulated isotopic ratios and dates (and the mean and median dates derived from them) are *all* corrected for common Pb, using the ^{204}Pb-correction method. Further, sample- and Group-specific details of the common Pb correction are given within each analytical data-table.

Dates derived from the pooling of multiple individual analyses are error-weighted means unless otherwise specified, and their uncertainties are quoted at the 95% confidence level unless otherwise indicated. Each error-weighted mean has a Mean Square of Weighted Deviates (MSWD) value, which is a measure of the degree of scatter of the constituent analyses relative to the assigned uncertainties (Ludwig, 2003), and an associated 'probability of equivalence' (P_{equiv}) value, which is the probability that the constituent analyses are equivalent within their uncertainties. By convention, scatter beyond the assigned uncertainties is assumed to be present when P_{equiv} is less than 0.05. In cases where P_{equiv} is equal to or greater than 0.05, but the MSWD value exceeds 1, the dispersion of the data-points beyond their analytical uncertainties is acknowledged by expanding the 95% confidence interval of the mean, via multiplication of its 1σ error firstly by Student's t for n - 1 degrees of freedom (where n is the number of constituent analyses), and secondly by the square root of the MSWD (Ludwig, 2003).

For clusters of analyses scattered beyond their assigned uncertainties ($P_{equiv} < 0.05$), robust means (e.g. Tukey's biweight mean: Hoaglin et al., 1983) were calculated as described in the text, and their uncertainties are quoted at the 95% confidence level unless otherwise indicated. Similarly, medians are quoted with non-parametric uncertainties at a confidence level of about 95% (Rock et al., 1987). All algorithms were utilised via the implementation of Ludwig (2003).

A.2.1. Calibration Procedures

Elemental U concentrations in the unknown zircons were calibrated using the M257 reference zircon (840 ppm U; Nasdala et al., 2008), and the power-law relationship proposed by Claoué-Long et al. (1995):

$$\left[{}^{196}Zr_2O^+/{}^{238}U^+\right] = A \times \left[{}^{254}UO^+/{}^{238}U^+\right]^{0.66} \qquad (1)$$

where A is a session-dependent constant determined from measurements on M257. All U concentration data tabulated for unknowns have uncertainties of the order of 15–20%, based on the extent of known variations in U abundance in M257.

Values of $^{232}Th/^{238}U$ in the unknown zircons were calculated using the relationship proposed by Williams et al. (1996):

$$^{232}Th/^{238}U = \left[{}^{248}ThO^+/{}^{254}UO^+\right] \times \left\{\left(0.03446 \times \left[{}^{254}UO^+/{}^{238}U^+\right]\right) + 0.868\right\} \qquad (2)$$

The values of $^{238}U/^{206}Pb$ in the unknowns were calibrated using one of two reference zircons: TEMORA2 ($^{238}U/^{206}Pb$ = 14.972, corresponding to an age of 416.8 Ma; Black et al., 2004) or AusZ2 ($^{238}U/^{206}Pb$ = 165.39, corresponding to an age of 38.86 Ma; A.K. Kennedy, personal communication 2012), in conjunction with a power-law relationship (Claoué-Long et al., 1995) of the form:

$$\left[{}^{206}Pb^+/{}^{238}U^+\right] = B \times \left[{}^{254}UO^+/{}^{238}U^+\right]^2 \qquad (3)$$

where B is a session-dependent constant determined from measurements on the $^{238}U/^{206}Pb$ reference zircon.

Each analytical session was monitored for long-term secular drift in the calibration defined by the reference zircon, via calculation of the slope of the robust regression of the individual $^{238}U/^{206}Pb$ dates (Ma) against the cumulative duration of the session at the time of acquisition (measured in hours since commencement). For session 120088, the 95% confidence interval of this slope encompasses zero, and no secular drift correction need be applied to the $^{238}U/^{206}Pb$ calibration. However, this is not the case for session 120071, and the secular drift correction applied is described in the next section.

The values of $^{207}Pb/^{206}Pb$ in the unknowns were monitored using the OG1 reference zircon ($^{207}Pb/^{206}Pb$ = 0.29907 ± 0.00011, corresponding to an age of 3465.4 ± 0.6 Ma; Stern et al., 2009). For each session, the error-weighted mean $^{207}Pb/^{206}Pb$ for OG1 (denoted $[^{207}Pb/^{206}Pb]_{OG1}$) was calculated (Appendix Table A.1), and the procedure of Stern et al. (2009) used to determine an instrumental mass fractionation (IMF) factor (α):

$$\alpha = [^{207}Pb/^{206}Pb]_{OG1} / 0.29907 \tag{4}$$

The dates corresponding to the session-specific $[^{207}Pb/^{206}Pb]_{OG1}$ values are summarised in Appendix Table A.1. In some geological scenarios (e.g. when comparing highly precise weighted mean $^{207}Pb/^{206}Pb$ dates from Archean and Paleoproterozoic rocks), it is desirable to perform session-specific standardisation of $^{207}Pb/^{206}Pb$ and propagate inter-session calibration uncertainties, as described in detail by Bodorkos et al. (2013). However, in the samples documented in this report, zircons of pre-Neoproterozoic age were rarely encountered, and the calculation of weighted mean $^{207}Pb/^{206}Pb$ dates was largely unnecessary. Uncertainties on individual $^{207}Pb/^{206}Pb$ analyses are governed by (relatively poor) counting statistics, and are large enough that both the instrumental mass fractionation correction and its associated uncertainty are rendered insignificant. Consequently, the tabulated values of $^{207}Pb/^{206}Pb$ for each sample have not been corrected for instrumental mass fractionation.

A.2.2. Propagation of Uncertainties

In each session, a 'calibration constant' value is determined for each individual analysis of the selected $^{238}U/^{206}Pb$ reference zircon (i.e. $b_i = [^{206}Pb^+/^{238}U^+]_i / [^{254}UO^+/^{238}U^+]_i^2$). Uncertainties associated with each of these individual 'calibration constants' (i.e. ± b_i) are governed primarily by the counting statistics associated with the constituent isotopic ratio(s). The value of the session 'calibration constant' (B; see equation (3)) is calculated as the error-weighted mean of the session-specific population of individual calibration constants. However, these populations commonly display significant excess scatter, manifested as an MSWD value for B that exceeds unity, despite most reference zircons being (by definition) characterised by $^{238}U/^{206}Pb$ homogeneity at a range of scales. This indicates that the values of ± b_i are usually underestimated from analysis to analysis. Consequently, for each session, SQUID calculates the constant additional uncertainty per spot (expressed as a percentage) that needs to be added in quadrature to each ± b_i value, in order to produce MSWD ~ 1 for the population of b_i values used to calculate B (Ludwig, 2009). This constant additional uncertainty is termed the 'spot-to-spot error', and its session-specific 2σ values are presented in Appendix Table A.1. The spot-to-spot error (also known as the 'within-session' error, the 'reproducibility', and the 'external' error) is added in quadrature to the other sources of error (principally related to counting statistics and the common Pb correction) for each value of $^{238}U/^{206}Pb$ in the unknowns, and thus is incorporated into the uncertainty of each individual $^{238}U/^{206}Pb$ value presented in the analytical data-tables.

For each session, SQUID also calculates an uncertainty for the session calibration constant (i.e. ± B) that takes into account the spot-to-spot error as well as the individual calibration constants and their uncertainties. This uncertainty is termed the 'session-to-session error', and its session-specific 2σ values are presented in Appendix Table A.1. The session-to-session error (also known as the 'between-session' error, the 'calibration uncertainty', and the 'error of the mean') is not included in the uncertainties of individual $^{238}U/^{206}Pb$ values presented in the analytical data-tables, and should be neglected when comparing error-weighted mean $^{238}U/^{206}Pb$ dates for unknowns co-analysed in a single analytical session. However, it must be accounted for when seeking to compare $^{238}U/^{206}Pb$ datasets more widely (e.g. between different analytical sessions), especially when calculating error-weighted mean $^{238}U/^{206}Pb$ dates for unknowns, because the session-to-session error can be of comparable magnitude to the 95% confidence interval arising from population statistics.

For example, calculating the magmatic crystallisation age of the Morobe Granodiorite (MRA 100417, GA 2131311) using the 27 $^{238}U/^{206}Pb$ dates in Group 1 (Table 3.2) yields a weighted mean date of 13.62 ± 0.11 Ma (i.e. an uncertainty of 0.82% at the 95% confidence level) based solely on the tabulated data. This uncertainty is appropriate for the purpose of direct comparison with the mean ages derived from the two Bulolo Volcanics samples, because the three samples were co-analysed and thus share a common calibration. However, when seeking to compare the magmatic crystallisation age of the Morobe Granodiorite with any other SHRIMP $^{238}U/^{206}Pb$ result (from this report or elsewhere), it is necessary to include (via quadratic addition) the relevant session-to-session error (0.55% (2σ) for session 120071; Appendix Table A.1), and the expanded uncertainty is given by $\text{sqrt}[(0.82\%)^2 + (0.55\%)^2] = 0.99\%$, which represents an absolute uncertainty of 0.13 Ma relative to a weighted mean of 13.62 Ma. Consequently, the magmatic crystallisation age of the Morobe Granodiorite is reported as 13.62 ± 0.13 Ma throughout this report, in order to maximise its comparability with existing (and future) geochronological determinations.

A.2.3. Discordance

Discordance is a measure of the internal agreement of the dates derived from the independent $^{207}Pb/^{206}Pb$ and $^{238}U/^{206}Pb$ isotopic systems, within a single analysis. In this report, it is applicable only to analyses that utilise the ^{204}Pb-correction for common Pb, as application of the ^{207}Pb-correction entails the explicit assumption of perfect agreement between the radiogenic $^{207}Pb/^{206}Pb$ and $^{238}U/^{206}Pb$ isotopic systems, which implies zero discordance.

In ^{204}Pb-corrected zircons of Mesoproterozoic and older age, discordance values for single analyses (and discordance patterns within a population of analyses) can provide important information about the timing and extent of post-crystallisation loss of radiogenic Pb (see Sircombe et al. (2007) and Carson et al. (2010) for more detailed discussion), and are often a valuable indicator of ‘geological’ data quality. The comparison is less useful in SHRIMP analyses of post-1000 Ma zircons, because the relatively poor counting statistics associated with their $^{207}Pb/^{206}Pb$ determinations usually result in uncertainties large enough to obscure the ‘true’ agreement or otherwise of the two isotopic systems. Nevertheless, the comparison has been performed (on analyses yielding Mesozoic or older dates) throughout this report, using the equation:

$$\text{Disc}\ (\%) = 100 \times \left[\left({}^{207}\text{Pb}/{}^{206}\text{Pb date}\right) - \left({}^{238}\text{U}/{}^{206}\text{Pb date}\right)\right] / \left({}^{238}\text{U}/{}^{206}\text{Pb date}\right) \qquad (5)$$

The analysis-specific results of equation (5) are reported (for ^{204}Pb-corrected analyses) in the analytical data-tables.

A.3. Session-Specific Calibrations and Data Reduction

The data reported herein were obtained over the course of two separate analytical sessions. Each session has its own calibration characteristics and data reduction parameters (Appendix Table A.1), and is described separately below.

A.3.1. Session 120071: Mount GA6211, 27 September–1 October 2012

This session encompassed the analysis of three samples:

- MRA 100214 (GA 2131308): Bulolo Volcanics ('bombs' of porphyritic andesite)
- MRA 100338 (GA 2131310): Bulolo Volcanics (subvolcanic diorite)
- MRA 100417 (GA 2131311): Morobe Granodiorite

Two $^{238}U/^{206}Pb$ reference zircons were analysed during session 120071: TEMORA2 (43 analyses) and AusZ2 (44 analyses). Unfortunately, instrument operating conditions did not remain stable throughout the session, with the TEMORA2 and AusZ2 datasets both illustrating an unambiguous trend toward lower $^{238}U/^{206}Pb$ dates as the session progressed (Appendix Figure A.1). For each reference zircon, the slope of the robust regression of the individual $^{238}U/^{206}Pb$ dates (Ma) against the cumulative duration of the session at the time of acquisition (measured in hours since commencement) was significantly more negative than zero at the 95% confidence level (Appendix Figure A.1), necessitating the application of a secular drift correction to the $^{238}U/^{206}Pb$ calibration.

The results of independently applying the secular drift corrections indicated in Appendix Figure A.1 are shown in Appendix Figure A.2. The TEMORA2 dataset shows less internal variation than the AusZ2 dataset (as evidenced by 2σ spot-to-spot errors of 1.41% and 2.48% respectively); nevertheless, AusZ2 was selected as the $^{238}U/^{206}Pb$ reference zircon for this session, because (i) the slope of its secular drift correction required is shallower than that of TEMORA2 (Appendix Figure A.1), and (ii) its low and relatively uniform ^{206}Pb count rates (50–68 counts/second) are much more closely matched to those of the Miocene and Pliocene magmatic zircons under investigation (3–48 counts/second across the three samples) than are the higher ^{206}Pb count rates obtained on TEMORA2 (147–1301 counts/second in session 120071). Once the secular drift correction is applied, all 44 AusZ2 analyses define a coherent calibration (Appendix Figure A.2): the weighted mean $^{238}U/^{206}Pb$ value has a session-to-session error of 0.55% (2σ), and a spot-to-spot error of 2.48% (2σ).

Common Pb corrections were performed using ^{207}Pb, and the accuracy of the drift-corrected AusZ2 calibration was verified by all 43 analyses of TEMORA2 (Appendix Figure A.3), which yielded a weighted mean $^{238}U/^{206}Pb$ date of 415.2 ± 1.8 Ma (95% confidence; MSWD = 0.35, P_{equiv} = 1.00). This result is indistinguishable from its reference $^{238}U/^{206}Pb$ age of 416.8 Ma (Black et al., 2004). In addition, 20 analyses of the $^{207}Pb/^{206}Pb$ reference zircon OG1 were obtained during session 120071 (Appendix Figure A.3). The weighted mean of all 20 $^{207}Pb/^{206}Pb$ dates is 3465.4 ± 1.8 Ma (MSWD = 0.91, P_{equiv} = 0.57), which is identical to the reference value, and no correction for instrumental fractionation of $^{207}Pb/^{206}Pb$ was applied.

A.3.2. Session 120088: Mount GA6211, 1–5 November 2012

This session encompassed the analysis of one sample:

- MRA 100211 (GA 2131307): Owen Stanley Metamorphics (metasandstone)

Forty-one analyses of the $^{238}U/^{206}Pb$ reference zircon TEMORA2 were obtained during session 120088. Instrument operating conditions were stable, with robust regression of the individual $^{238}U/^{206}Pb$ dates (Ma) against the cumulative duration of the session at the time of acquisition yielding a slope of -0.022 +0.043/-0.040 Ma/hour (95% confidence). This indicates that no secular drift in the $^{238}U/^{206}Pb$ calibration is resolvable at the scale of the total session duration.

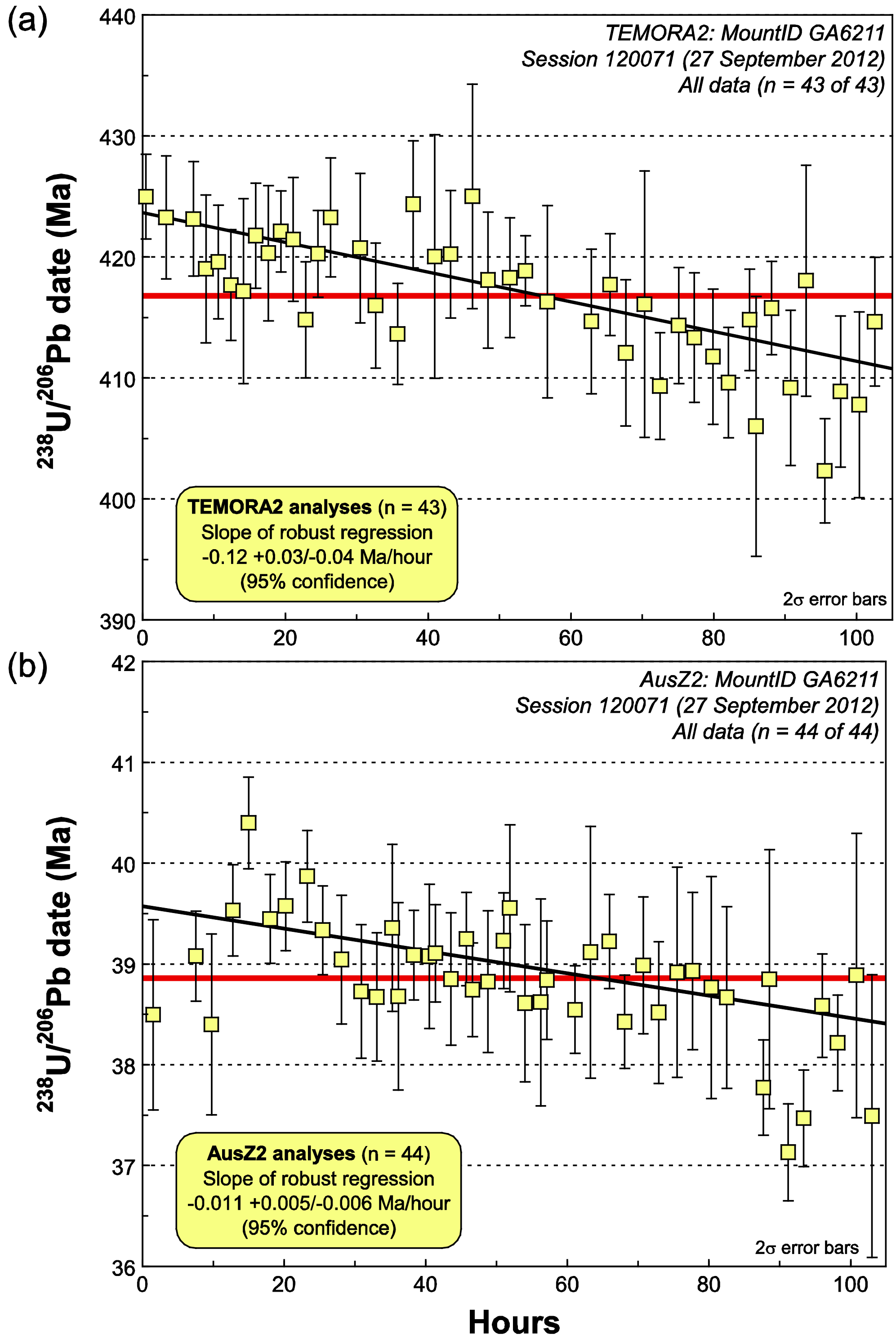

Appendix Figure A.1 *SHRIMP data for the two $^{238}U/^{206}Pb$ reference zircons analysed during session 120071, illustrating the existence of measurable drift of the $^{238}U/^{206}Pb$ calibration as the session progressed. (a) TEMORA2 $^{238}U/^{206}Pb$ dates as a function of session duration; (b) AusZ2 $^{238}U/^{206}Pb$ dates as a function of session duration. Pale yellow fill denotes analyses included in the respective calibrations. Heavy red lines denote reference values for TEMORA2 ($^{238}U/^{206}Pb$ date = 416.8 Ma) and AusZ2 ($^{238}U/^{206}Pb$ date = 38.86 Ma). Heavy black lines: robust regressions of individual $^{238}U/^{206}Pb$ dates against session duration.*

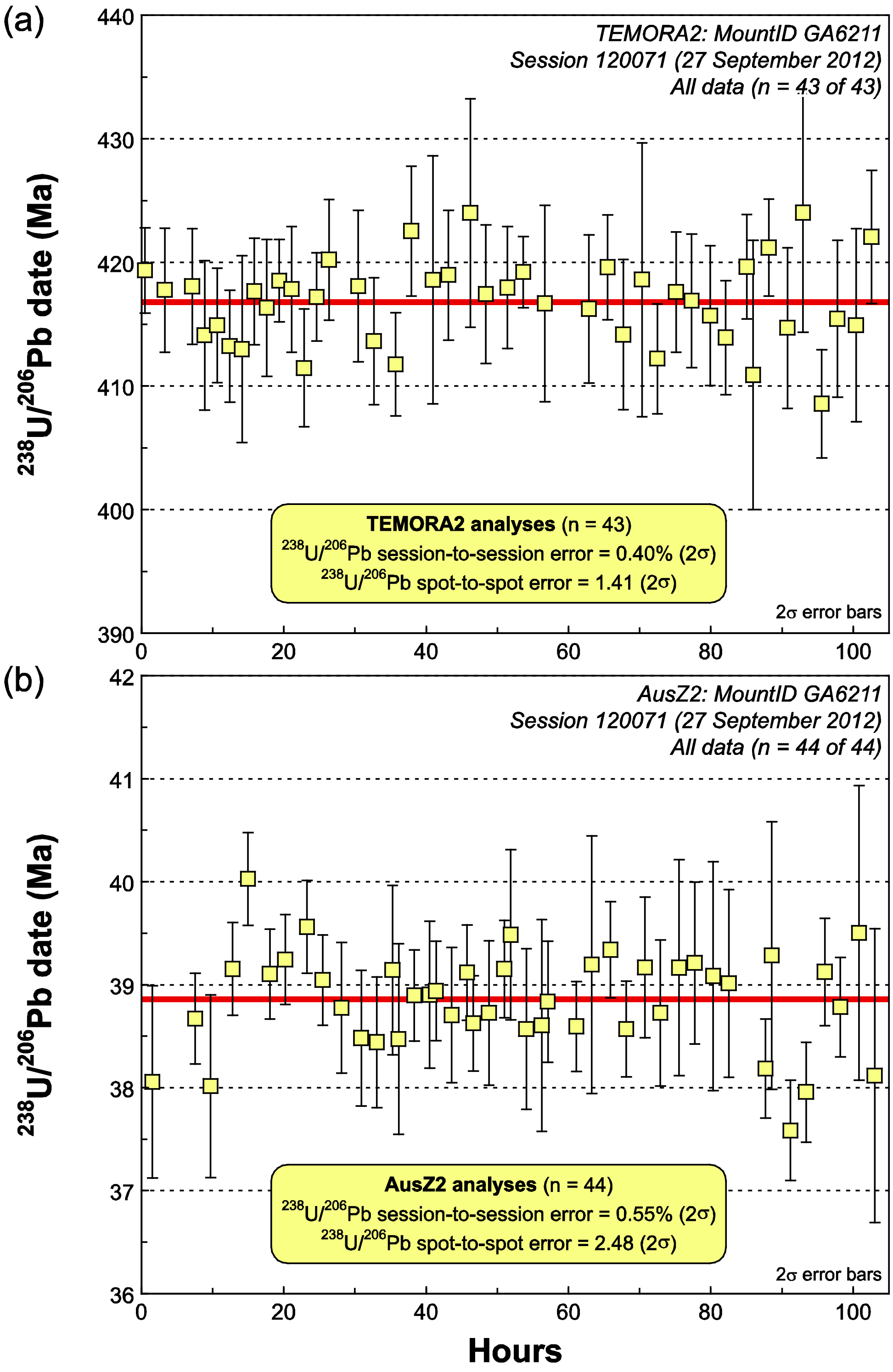

Appendix Figure A.2 *SHRIMP data for the two $^{238}U/^{206}Pb$ reference zircons analysed during session 120071, with each dataset independently corrected for secular drift. (a) TEMORA2 $^{238}U/^{206}Pb$ dates; (b) AusZ2 $^{238}U/^{206}Pb$ dates. Pale yellow fill denotes analyses included in the respective calibrations. Heavy red lines denote reference values for TEMORA2 ($^{238}U/^{206}Pb$ date = 416.8 Ma) and AusZ2 ($^{238}U/^{206}Pb$ date = 38.86 Ma).*

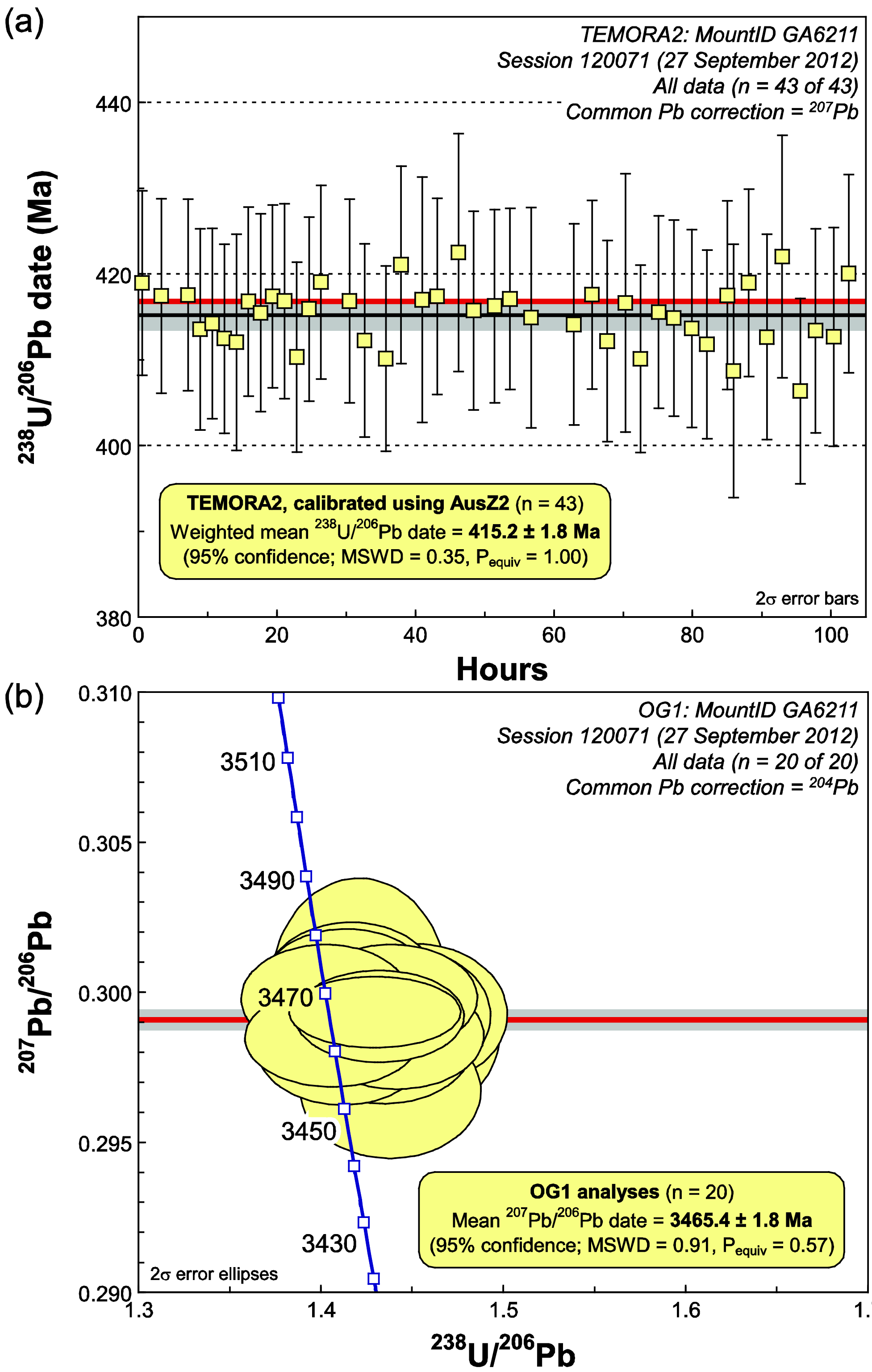

Appendix Figure A.3 *SHRIMP U-Pb data for reference zircons analysed during session 120071. (a) AusZ2-calibrated TEMORA2 $^{238}U/^{206}Pb$ dates in order of acquisition; (b) Tera-Wasserburg concordia diagram for OG1 data. Pale yellow fill denotes analyses included in the respective means. Heavy red lines denote reference values for TEMORA2 ($^{238}U/^{206}Pb$ date = 416.8 Ma) and OG1 ($^{207}Pb/^{206}Pb$ = 0.29907). Heavy black lines (obscured by heavy red line in lower panel) and grey bands: measured weighted mean and its 95% confidence interval, respectively.*

All 41 TEMORA2 analyses define a coherent calibration (Appendix Figure A.4): the weighted mean $^{238}U/^{206}Pb$ value has a session-to-session error of 0.22% (2σ), and a spot-to-spot error of 0.81% (2σ). However, this spot-to-spot error value is significantly lower than that usually derived from $^{238}U/^{206}Pb$ reference zircon datasets measured via SHRIMP, which raises the possibility that the value for session 120088 is underestimated. Consequently, the spot-to-spot error for session 120088 was increased to a nominal value of 1.50% (2σ) prior to its incorporation into the uncertainties of $^{238}U/^{206}Pb$ in the co-analysed unknowns, based on (i) the recommendations of Stern and Amelin (2003) regarding unaccounted variation in $^{238}U/^{206}Pb$ measurements via SHRIMP, modified by (ii) the consistent behaviour of TEMORA2 when analysed by the GA SHRIMP IIe, as documented by Bodorkos et al. (in press).

Common Pb corrections were performed using ^{204}Pb, and the possibility of overcounts at mass ^{204}Pb was monitored by reference to the robust mean of the 41 $^{207}Pb/^{206}Pb$ dates determined for TEMORA2 (415 ± 29 Ma). This result does not differ significantly from the reference value at the 95% confidence level, and ^{204}Pb overcounts based on measured ^{207}Pb and measured ^{208}Pb both yielded robust mean values indistinguishable from zero (+0.002 ± 0.024 and +0.028 ± 0.028 counts/second, respectively), so no correction was necessary.

In addition, 20 analyses of the $^{207}Pb/^{206}Pb$ reference zircon OG1 were obtained during session 120088. The weighted mean of all 20 $^{207}Pb/^{206}Pb$ dates is 3467.4 ± 1.4 Ma (MSWD = 0.83, P_{equiv} = 0.67), and although this very slightly exceeds the reference value at the 95% confidence level (Appendix Figure A.4), the measured instrumental mass fractionation correction and its associated uncertainty are both insignificant compared to the uncertainties on the individual $^{207}Pb/^{206}Pb$ analyses obtained during session 120088. Consequently, the tabulated values of $^{207}Pb/^{206}Pb$ for the sample have not been corrected for instrumental mass fractionation.

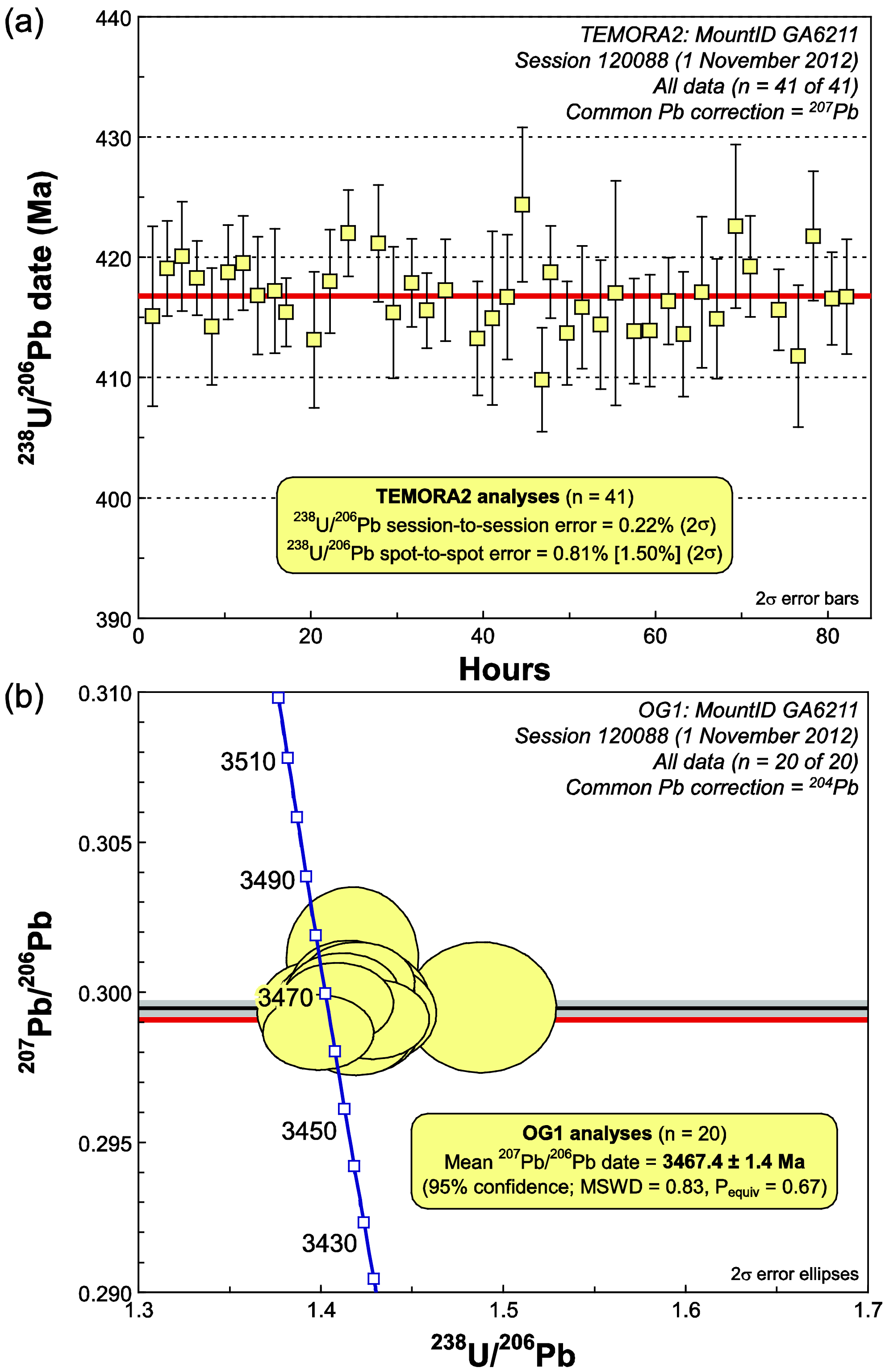

Appendix Figure A.4 *SHRIMP U-Pb data for reference zircons during session 120088. (a) TEMORA2 $^{238}U/^{206}Pb$ dates in order of acquisition; (b) Tera-Wasserburg concordia diagram for OG1 data. Pale yellow fill denotes analyses included in the respective calibrations. Heavy red lines denote reference values for TEMORA2 ($^{238}U/^{206}Pb$ date = 416.8 Ma) and OG1 ($^{207}Pb/^{206}Pb$ = 0.29907). Heavy black line and grey band: mean of measured $^{207}Pb/^{206}Pb$ and its 95% confidence interval, respectively.*